energies

MDPI

Article

Surface Permanent Magnet Synchronous Motors' Passive Sensorless Control: A Review

Alessandro Benevieri, Lorenzo Carbone, Simone Cosso, Krishneel Kumar, Mario Marchesoni *, Massimiliano Passalacqua and Luis Vaccaro

Electrical, Electronics and Telecommunication Engineering and Naval Architecture Department (DITEN), University of Genova, Via all'Opera Pia 11a, 16145 Genova, Italy
* Correspondence: marchesoni@unige.it

Abstract: Sensorless control of permanent magnet synchronous motors is nowadays used in many industrial, home and traction applications, as it allows the presence of a position sensor to be avoided with benefits for the cost and reliability of the drive. An estimation of the rotor position is required to perform the field-oriented control (FOC), which is the most common control scheme used for this type of motor. Many algorithms have been developed for this purpose, which use different techniques to derive the rotor angle from the stator voltages and currents. Among them, the so-called passive methods have gained increasing interest as they do not introduce additional losses and current distortion associated instead with algorithms based on the injection of high-frequency signals. The aim of this paper is to present a review of the main passive sensorless methods proposed in the technical literature over the last few years, analyzing their main features and principles of operation. An experimental comparison among the most promising passive sensorless algorithms is then reported, focusing on their performance in the low-speed operating region.

Keywords: permanent magnet synchronous motors (PMSM); sensorless control; review

Citation: Benevieri, A.; Carbone, L.; Cosso, S.; Kumar, K.; Marchesoni, M.; Passalacqua, M.; Vaccaro, L. Surface Permanent Magnet Synchronous Motors' Passive Sensorless Control: A Review. *Energies* **2022**, *15*, 7747. https://doi.org/10.3390/en15207747

Academic Editor: Valery Vodovozov

Received: 30 September 2022
Accepted: 17 October 2022
Published: 19 October 2022

1. Introduction

In recent decades, the use of the permanent magnet synchronous motor (PMSM) has become increasingly widespread, both for medium-power industrial applications and for electric traction drives. This type of motor is characterized by a high power density, high efficiency and good dynamic performance; it also has a high ratio between torque and inertia and can be controlled using relatively simple algorithms. The most commonly used control scheme for the PMSM is the field-oriented control (FOC), which operates in the synchronously rotating reference frame and makes use of PI regulators to control the d and q axis currents. For this reason, accurate information about the rotor position and the rotor speed at every instant is needed. These quantities are traditionally obtained using a position sensor mounted on the rotor shaft, such as an encoder or a resolver. However, position sensors have a high cost and worsen the reliability of the drive, as well as its dimensions. The solution that allows the use of a position sensor to be avoided consists of estimating the rotor position through a dedicated algorithm, starting from quantities such as stator currents and reference voltages. A large number of sensorless algorithms for PMSM have been presented and studied over the past few years, which use a large variety of different techniques to estimate the rotor angle.

The effectiveness of sensorless algorithms for PMSM is different depending on whether they are used for a surface mount PMSM (SPMSM) or an internal PMSM (IPMSM). In an IPMSM, the magnets are positioned in housings obtained in the rotor iron and this, therefore, generates a significant magnetic anisotropy, which results in a value of the inductance of the quadrature axis L_q different from that of the direct axis L_d. This magnetic saliency can be exploited to extract information about the rotor position more easily. Conversely,

in an SPMSM the magnets are mounted on the rotor surface, which is therefore almost magnetically isotropic (L_d is almost equal to L_q). For this type of motor, it is naturally more difficult to estimate the rotor position. The difference explained so far is schematized in Figure 1.

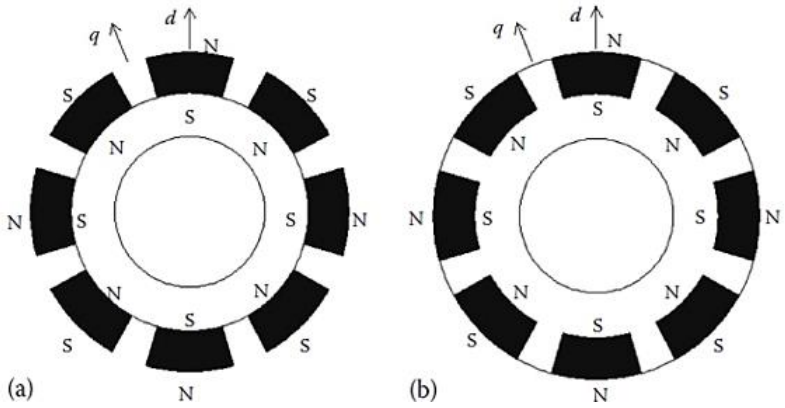

Figure 1. Structure of an SPMSM rotor (**a**) and of an IPMSM rotor (**b**).

Two large families of sensorless algorithms can be found in the technical literature. The first family is one of high-frequency injection algorithms, also called active algorithms or saliency-based algorithms [1–12]. Their operating principle is based on the injection of high-frequency voltage signals, superimposed on the stator supply voltages. Thanks to the magnetic saliency of the rotor, the amplitude of the resulting high-frequency currents on the two different reference axes depends on the rotor position, which can be estimated by demodulating and analyzing the resulting signals properly. As can be easily deduced, these methods are more suitable for IPMSM due to their high saliency. Active sensorless algorithms are also effective at low speed and zero speed, therefore they can be used for starting the motor from standstill [5–7]. However, the injection of high-frequency signals causes several drawbacks, such as additional losses, acoustic noise and an increase in current total harmonic distortion (THD) [8]. These problems become even more relevant in the case of SPMSMs because their low saliency makes it necessary to inject higher voltages to obtain an acceptable signal-to-noise ratio (SNR). A solution to this problem was proposed in [9].

The drawbacks associated with high-frequency injection can be overcome with the second family of sensorless algorithms, the so-called passive methods. These algorithms obtain the rotor position starting from the measurement of the stator currents and the reference voltages, without using additional injected signals. Passive algorithms can be further divided into two main classes: back-EMF algorithms and rotor flux observers (RFOs). The former derives the rotor position by estimating the back-EMFs of the motor in the stationary or in the rotating reference frame. This can be achieved with various techniques presented in the literature [13–37]. Some recently studied algorithms treat the back-EMFs as unknown external disturbances and estimate them using linear disturbance observers [16–21]. A back-EMF estimation method based on active damping techniques is presented in [22]. However, one of the most common back-EMF methods is represented by the sliding mode observer (SMO) [23–37]. The main advantage of SMO observers is their robustness, but the sliding mode switching function that is always present in these algorithms causes chattering problems and a consequent high noise in the estimation process. Various studies proposed partial solutions to this problem by substituting the traditional signum switching function typical of an SMO with others, such as the saturation function [29], the arcsine function [30], the sigmoid function [31–33] or the super-twisting function [34–36]. A comparison among different switching functions on the same SMO can be found in [37]. It should be mentioned that in a PMSM, the magnitude of the back-EMFs is directly proportional to the rotor speed. As a consequence, their effectiveness decreases

significantly at low speed and they cannot theoretically be used to start the motor from standstill. Unlike the back-EMF-based methods, RFOs are a class of passive algorithms that directly estimate the rotor flux angle. Since the flux is present even at standstill thanks to the presence of the permanent magnet, they can theoretically also operate at lower speeds. Some observers based on an extended or unscented Kalman filter were developed for this purpose [38–41]. A nonlinear rotor flux observer was presented in [42], and its validity was demonstrated in [43] with experimental tests. A new RFO designed to also work with SPMSMs was proposed by Bobtsov et al. in [44]. It is based on a linear regression algorithm that makes use of a highpass filter to reduce the effect of DC disturbances, and it was then improved by Choi et al. in [45] adding a feedback loop that compensates uncertainties of the motor parameters. The validity of this observer was demonstrated with experimental tests carried out in various load conditions in [46–48], and the tuning process of its parameters was studied in [49]. The same authors also developed another algorithm based on a regression model [50,51], made specifically for IPMSMs but adaptable for use with SPMSMs. Other types of rotor flux observers were proposed in [52,53].

Given the great variety of passive sensorless algorithms presented in recent years, the aim of this paper is to present a review of the main methods, analyzing their operating principles and their characteristics. This article is structured as follows. In Section 2 the model of a generic PMSM both in the stationary and rotating reference frame is presented and the structure of the most used FOC scheme is introduced. Section 3 is dedicated to back-EMF algorithms, while in Section 4 the most promising RFOs taken from the technical literature are reviewed. Finally, Section 5 describes some criteria by which the choice of a sensorless algorithm can be made, and presents the results of an experimental comparison carried out in [54] among five different algorithms, chosen from the most recent ones. The experimental tests presented in that work are performed on an SPMSM using the same test bench, focusing on the region of low-speed operation, which is generally the most critical for passive sensorless algorithms.

2. PMSM Model and FOC Scheme

2.1. Model of the PMSM

A generic three-phase PMSM can be modeled through the diagram shown in Figure 2 [20]. In that diagram, axes α-β constitute the stationary reference frame, axes *d*-*q* constitute the synchronously rotating reference frame and axes γ-δ constitute the estimated synchronous frame, which is used by some sensorless algorithms.

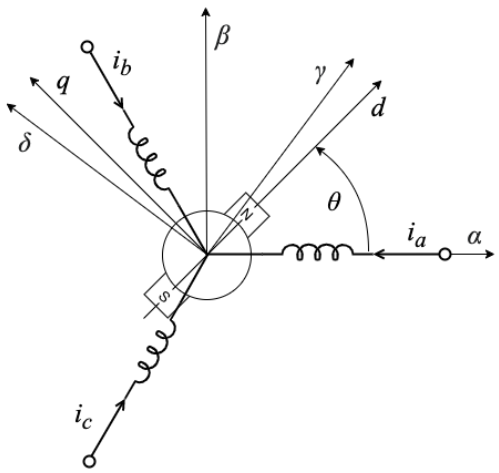

Figure 2. PMSM model in stationary and rotating reference frame.

In the stationary reference frame, the electrical equations of a PMSM can be expressed as in (1)

$$\begin{bmatrix} v_\alpha \\ v_\beta \end{bmatrix} = R_s \begin{bmatrix} i_\alpha \\ i_\beta \end{bmatrix} + p\left(\begin{bmatrix} L_s + \frac{\Delta L}{2}\cos 2\theta & \frac{\Delta L}{2}\sin 2\theta \\ \frac{\Delta L}{2}\sin 2\theta & L_s - \frac{\Delta L}{2}\cos 2\theta \end{bmatrix} \begin{bmatrix} i_\alpha \\ i_\beta \end{bmatrix} \right) + \begin{bmatrix} e_\alpha \\ e_\beta \end{bmatrix} \quad (1)$$

where v_α, v_β are the stator voltages, i_α, i_β are the stator currents, θ is the angle of the rotor flux, R_s is the stator resistance, L_d and L_q are the d and q axis inductances, respectively, $L_s = (L_d + L_q)/2$ and $\Delta L = (L_d - L_q)$. Moreover, e_α, e_β are the back-EMF, which can be expressed as in (2)

$$\begin{bmatrix} e_\alpha \\ e_\beta \end{bmatrix} = p\left(\varphi_m \begin{bmatrix} \cos\theta \\ \sin\theta \end{bmatrix} \right) = \omega\varphi_m \begin{bmatrix} -\sin\theta \\ \cos\theta \end{bmatrix} \quad (2)$$

where φ_m is the flux linkage constant and ω is the rotor angular speed. For an SPMSM, the conditions $L_d = L_q = L_s$ and $\Delta L = 0$ are true and the electrical equations can be simplified as in (3).

$$\begin{bmatrix} v_\alpha \\ v_\beta \end{bmatrix} = \begin{bmatrix} R_s + pL_s & 0 \\ 0 & R_s + pL_s \end{bmatrix} \begin{bmatrix} i_\alpha \\ i_\beta \end{bmatrix} + \begin{bmatrix} e_\alpha \\ e_\beta \end{bmatrix} \quad (3)$$

In the synchronously rotating reference frame, the electrical equations can be expressed as in (4)

$$\begin{bmatrix} v_d \\ v_q \end{bmatrix} = \begin{bmatrix} R_s + pL_d & -\omega L_q \\ \omega L_d & R_s + pL_q \end{bmatrix} \begin{bmatrix} i_d \\ i_q \end{bmatrix} + \begin{bmatrix} 0 \\ \omega\varphi_m \end{bmatrix} \quad (4)$$

where v_d, v_q are the stator voltages and i_d, i_q are the stator currents. Additionally here, for an SPMSM, $L_d = L_q = L_s$ can be assumed.

2.2. Field-Oriented Control Scheme

The well-known FOC scheme used for PMSM control in the case of sensorless operation is shown in Figure 3.

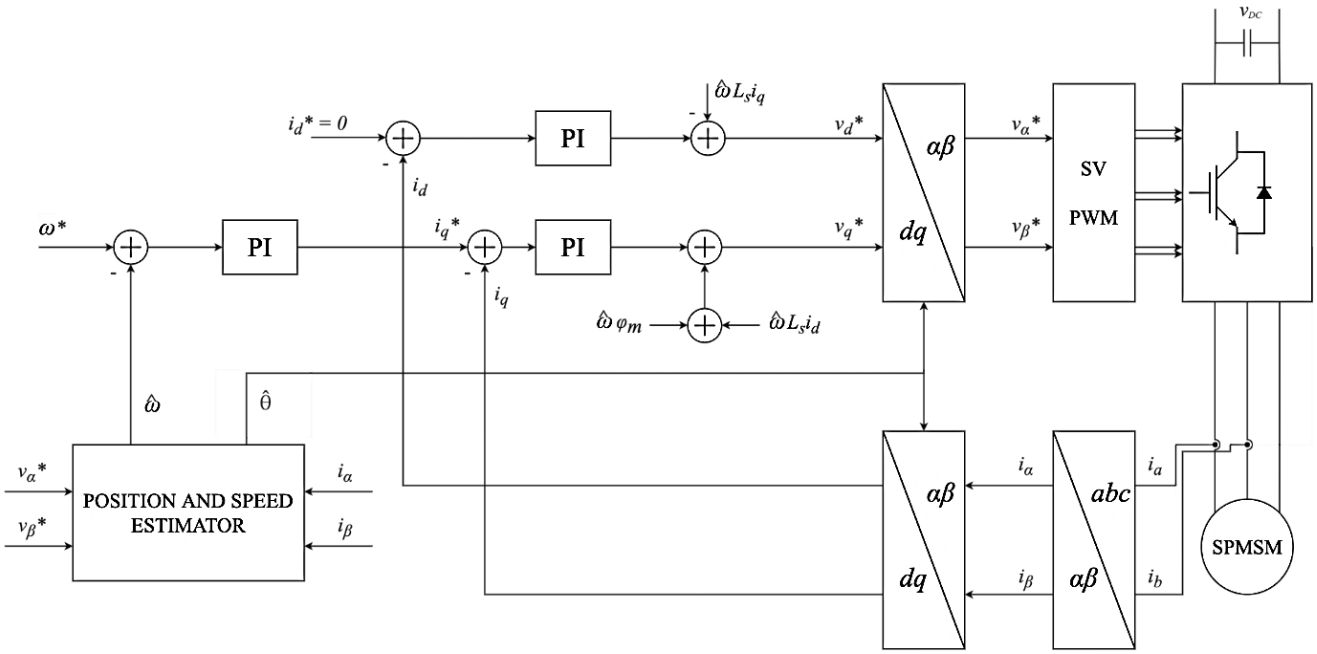

Figure 3. Sensorless FOC control scheme for PMSM.

Note that in the scheme, reference quantities are noted with *, estimated quantities are noted with ˆ and measured quantities are indicated without symbols. To estimate the rotor speed $\hat{\omega}$, it would theoretically be sufficient to derive the estimated position with respect to

time. However, this would amplify the high-frequency content of the signal and generate additional noise. Therefore, a commonly adopted solution [43–49] is to use a dedicated phase-locked loop (PLL), whose scheme is shown in Figure 4.

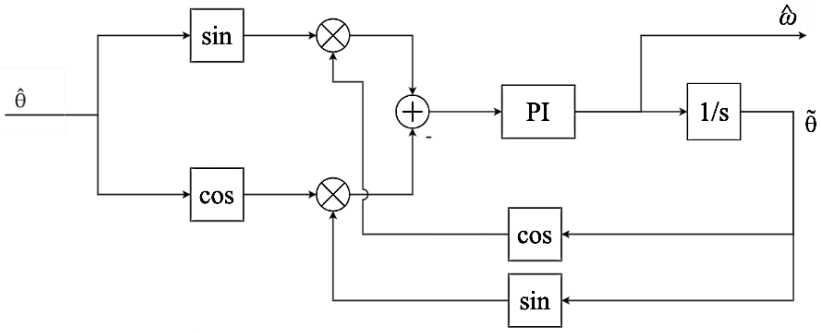

Figure 4. PLL commonly used for speed estimation.

3. Back-EMF-Based Sensorless Algorithms

As mentioned in the introduction, this class of sensorless algorithms derives the rotor angle starting from an estimation of the motor back-EMFs. Two different methods based on back-EMF estimation are described in this section. The first one is a linear disturbance observer, while the second one is a sliding mode observer.

3.1. Sensorless Algorithm Based on Linear Disturbance Observer

The operating principle of this algorithm consists of observing the so-called extended back-EMFs of the motor, which can be defined both in the synchronous and in the stationary reference frame, by means of disturbance observers. For simplicity, only the analysis of the algorithm developed in the synchronous reference frame [20,21] is reported here. The first step is to rewrite the electrical equations expressed in (4) as follows

$$\begin{bmatrix} v_d \\ v_q \end{bmatrix} = \begin{bmatrix} R_s + pL_d & -\omega L_q \\ \omega L_q & R_s + pL_d \end{bmatrix} \begin{bmatrix} i_d \\ i_q \end{bmatrix} + \begin{bmatrix} 0 \\ E_{ex} \end{bmatrix} \tag{5}$$

in which the extended back-EMF E_{ex} is highlighted, which can be expressed as in (6)

$$E_{ex} = (L_d - L_q)(\omega i_d - p i_q) + \omega \varphi_m \tag{6}$$

Since the rotor angle, which coincides with the angle of the synchronous reference frame, is unknown, the equations have to be expressed in an estimated synchronous frame γ-δ oriented on the estimated angle $\hat{\theta}$ as in (7)

$$\begin{bmatrix} v_\gamma \\ v_\delta \end{bmatrix} = \begin{bmatrix} R_s + pL_d & -\hat{\omega} L_q \\ \hat{\omega} L_q & R_s + pL_d \end{bmatrix} \begin{bmatrix} i_\gamma \\ i_\delta \end{bmatrix} + \begin{bmatrix} e_\gamma \\ e_\delta \end{bmatrix} \tag{7}$$

Under the assumption that the estimated speed $\hat{\omega}$ is almost equal to ω, the back-EMFs e_γ, e_δ can be approximated as in (8)

$$\begin{bmatrix} e_\gamma \\ e_\delta \end{bmatrix} = E_{ex} \begin{bmatrix} -\sin \Delta\theta \\ \cos \Delta\theta \end{bmatrix} \tag{8}$$

in which $\Delta\theta$ is the position estimation error defined as in (9)

$$\Delta\theta = \hat{\theta} - \theta \tag{9}$$

The operation of the algorithm is based on the consideration that, as it can be deduced from (8), the extended back-EMFs contain the information about the estimated position

error. Note that if the position is correct, the γ component of the back-EMF is equal to zero. Therefore, the rotor angle can be estimated by means of a PLL that aims to keep $e_\gamma = 0$.

In order to use disturbance observers in the estimation process, the PMSM equations in the estimated synchronous frame have to be rewritten in a scalar form as in (10)

$$\begin{cases} pi_\gamma = v_\gamma / L_d + f_\gamma + f_{e\gamma} + f_{i\gamma} \\ pi_\delta = v_\delta / L_d + f_\delta + f_{e\delta} + f_{i\delta} \end{cases} \tag{10}$$

where:

- f_γ and f_δ represent the known model quantities since they are expressed as a function of the motor parameters, currents and speed as in (11)

$$\begin{cases} f_\gamma = \frac{\hat{\omega} L_q i_\delta}{L_d} - \frac{R_s i_\gamma}{L_d} \\ f_\delta = -\frac{\hat{\omega} L_q i_\gamma}{L_d} - \frac{R_s i_\delta}{L_d} \end{cases} \tag{11}$$

- $f_{e\gamma}$ and $f_{e\delta}$ represent the unknown external disturbances as they are expressed as a function of the back-EMFs as in (12)

$$\begin{cases} f_{e\gamma} = -\frac{e_\gamma}{L_d} \\ f_\delta = -\frac{e_\delta}{L_d} \end{cases} \tag{12}$$

- $f_{i\gamma}$ and $f_{i\delta}$ represent the unknown internal disturbances, which are caused by uncertainties in the motor parameters. They are expressed as a function of ΔR_s, ΔL_d, ΔL_q and $\Delta \varphi_m$, which are the variations of the real parameters R_s, L_d, L_q and φ_m with respect to their nominal value.

The external and internal disturbances thus defined can be estimated by means of the so-called Linear Extended State Observers (LESOs). The LESOs that are usually employed for this type of sensorless algorithm, both in the stationary and in the rotating reference frame, estimate the desired quantities by evaluating the difference between the estimated and measured stator currents. A possible implementation of the LESO for external disturbance estimation in the γ-δ frame, referring to the case described above, is reported in (13)

$$\begin{cases} p\hat{i}_\gamma = v_\gamma / L_d + f_\gamma + \hat{f}_{e\gamma} - L_{\gamma 1}\varepsilon_\gamma \\ p\hat{f}_{e\gamma} = -L_{\gamma 2}\varepsilon_\gamma \\ p\hat{i}_\delta = v_\delta / L_d + f_\delta + \hat{f}_{e\delta} - L_{\delta 1}\varepsilon_\delta \\ p\hat{f}_{e\delta} = -L_{\delta 2}\varepsilon_\delta \end{cases} \tag{13}$$

where $\hat{i}_\gamma$ and $\hat{i}_\delta$ are the estimated currents, $\varepsilon_\gamma = \hat{i}_\gamma - i_\gamma$ and $\varepsilon_\delta = \hat{i}_\delta - i_\delta$ are the current estimation errors, $\hat{f}_{e\gamma}$ and $\hat{f}_{e\delta}$ are the estimated external disturbances and $L_{\gamma 1}$, $L_{\delta 1}$, $L_{\gamma 2}$, $L_{\delta 2}$ are the LESO gains.

The performance of the algorithm described above has been evaluated experimentally in [21]. The scheme of implementation of the algorithm is shown in Figure 5. Tests results show a good performance of the algorithm both in steady state operation, with and without a mismatch in the PMSM parameters and during transients such as a sudden load torque step at constant speed.

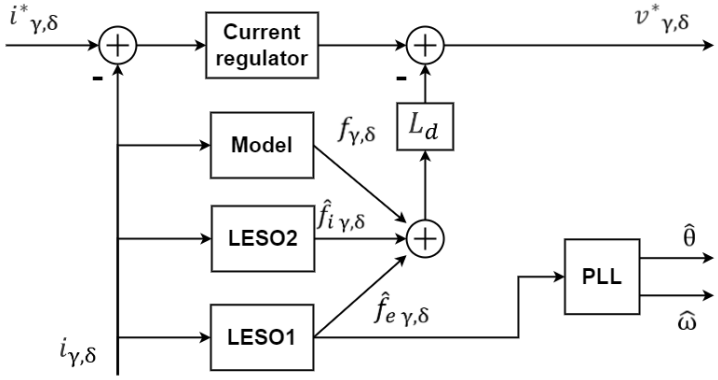

Figure 5. Implementation scheme of sensorless control based on linear disturbance observers in [21].

3.2. Sliding Mode Observer

The variety of sliding mode sensorless algorithms proposed in the literature in recent years is very large. Like other types of algorithms based on sliding mode, they are generally characterized by a strong robustness against parameter variations since the variables that constitute the considered state space are forced to stay on a chosen trajectory by means of a sliding mode switching function. However, this results in the presence of a chattering phenomenon that introduces additional noise in the estimation process. Various techniques have been proposed to minimize this effect [29–36]. The most widely used operating principle of a sliding mode position observer including common solutions to the chattering problem is described below, considering its application in the stationary reference frame and under the hypothesis of an isotropic rotor (SPMSM).

The electrical equations in (3) can be rearranged as in (14)

$$p\begin{bmatrix} i_\alpha \\ i_\beta \end{bmatrix} = -\frac{R_s}{L_s}\begin{bmatrix} i_\alpha \\ i_\beta \end{bmatrix} + \frac{1}{L_s}\begin{bmatrix} v_\alpha - e_\alpha \\ v_\beta - e_\beta \end{bmatrix} \tag{14}$$

in which the back-EMFs e_α, e_β contain the information about the rotor position. An expression for the stator currents estimated by the SMO can be derived from the previous equation as in (15)

$$p\begin{bmatrix} \hat{i}_\alpha \\ \hat{i}_\beta \end{bmatrix} = -\frac{R_s}{L_s}\begin{bmatrix} \hat{i}_\alpha \\ \hat{i}_\beta \end{bmatrix} + \frac{1}{L_s}\begin{bmatrix} v_\alpha - z_\alpha \\ v_\beta - z_\beta \end{bmatrix} \tag{15}$$

where the measured currents have been substituted by the estimated ones and the back-EMFs have been substituted by the sliding mode control functions z_α, z_β, which can be defined as in (16) referring to a basic SMO scheme

$$\begin{bmatrix} z_\alpha \\ z_\beta \end{bmatrix} = k\begin{bmatrix} sgn\left(\hat{i}_\alpha - i_\alpha\right) \\ sgn\left(\hat{i}_\beta - i_\beta\right) \end{bmatrix} \tag{16}$$

where k is the switching gain. The chosen sliding mode surface can be described by the condition in (17)

$$\begin{bmatrix} \left(\hat{i}_\alpha - i_\alpha\right) \\ \left(\hat{i}_\beta - i_\beta\right) \end{bmatrix} = \begin{bmatrix} 0 \\ 0 \end{bmatrix} \tag{17}$$

When this happens and the system is operating in sliding mode, taking into account (14) and (15), the condition in (18) is realized

$$\begin{bmatrix} z_\alpha \\ z_\beta \end{bmatrix} \approx \begin{bmatrix} e_\alpha \\ e_\beta \end{bmatrix} \tag{18}$$

Therefore, the control functions z_α, z_β approximate the back-EMFs and can be used to extract the information about the rotor position by means of a common PLL. In order to do this, however, they have to be filtered since they contain a strong high-frequency

component due to the presence of the switching function. In most cases, a lowpass filter or a more sophisticated filter is used to obtain the estimated back-EMFs $\hat{e}_\alpha$, $\hat{e}_\beta$. Finally, the estimated position and speed can be derived from the back-EMFs by means of a PLL. The structure of a generic SMO position estimator is shown in Figure 6.

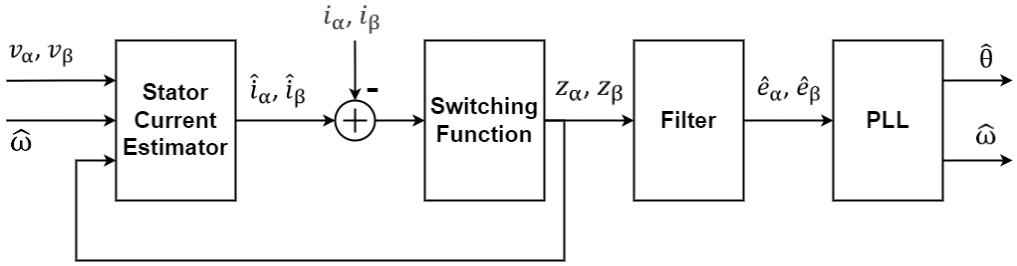

Figure 6. Basic SMO scheme.

As mentioned before, the reduction in the high-frequency content in the estimated back-EMFs, with the aim to improve the effectiveness of the estimator, has been the object of many studies [29–36]. This can be carried out essentially by acting on two aspects of the scheme:

- The selection of the most suitable switching function, which must be chosen among those functions that approximate the behavior of the signum function used in the basic scheme but generate a lower high-frequency content.
- The adoption of the most effective filter, replacing the traditionally used lowpass filter, which introduces a phase shift, resulting in a delay in the estimation process.

With regard to the switching function, the most studied alternatives in technical literature are the following:

- The traditional signum function (16), shown in Figure 7a, which is the easiest to be implemented but generates the worst signal spectrum in terms of high-frequency content.
- The saturation function [29], shown in Figure 7b. It can be expressed for generic variables x, y as in (19)

$$\begin{cases} y = k\ x > E_{max} \\ y = \left(\frac{k}{E_{max}}\right) x\ |x| < E_{max} \\ y = -k\ x < -E_{max} \end{cases} \tag{19}$$

  where k is the switching gain and E_{max} is a parameter.
- The sigmoid function [31–33] is shown in Figure 7c. It can be expressed as in (20)

$$y = k\left[\left(\frac{2}{1+e^{-ax}}\right) - 1\right] \tag{20}$$

  where k is the switching gain and a is a parameter.
- A possible alternative to the previous functions is the super-twisting algorithm [34–36]. Unlike the previous ones, it does not consist of a simple function but of a control law obtained by inserting the signum function into an integral filter. The resulting expression for z_α, z_β is given by (21), where k_1, k_2 are the two gains

$$\begin{bmatrix} z_\alpha \\ z_\beta \end{bmatrix} = \begin{bmatrix} k_1 \left|\hat{i}_\alpha - i_\alpha\right|^{\frac{1}{2}} sgn\left(\hat{i}_\alpha - i_\alpha\right) + k_2 \int sgn\left(\hat{i}_\alpha - i_\alpha\right) dt \\ k_1 \left|\hat{i}_\beta - i_\beta\right|^{\frac{1}{2}} sgn\left(\hat{i}_\beta - i_\beta\right) + k_2 \int sgn\left(\hat{i}_\beta - i_\beta\right) dt \end{bmatrix} \tag{21}$$

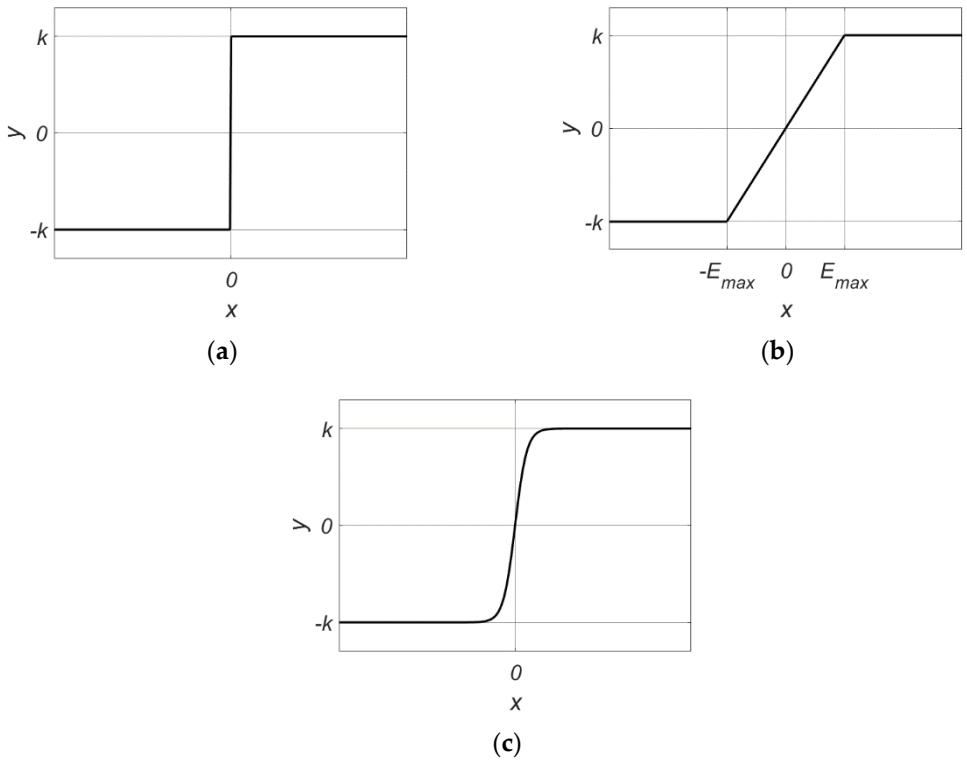

Figure 7. Possible switching function that can be used in the SMO algorithm: (**a**) signum function; (**b**) saturation function; (**c**) sigmoid function.

In [37] a comparison among the first three switching functions mentioned above is carried out with simulations and experimental tests. All the switching functions were implemented in the same SMO scheme to establish which is the most suitable one. The estimated back-EMFs and the estimated position error were evaluated for each case. Results showed that the high-frequency ripple in the estimated back-EMFs and the angle error are both reduced using the saturation function with respect to the signum function, but a quite high chattering phenomenon is still observed during some transients. Using the sigmoid function leads to a further improvement, giving the best results in terms of estimation effectiveness and high-frequency content in the observed back-EMFs.

Another solution to reduce the chattering problem is studied in [25] for PMSM drives with a small DC link capacitor. It is called Fast Sliding Mode Observer (FSMO), as it basically consists of executing the estimation algorithm iteratively four times in one current control cycle so that the phase delay and the ripples in the estimation of the back-EMF are minimized. This obviously leads to a more intensive computational effort.

In most cases, it is still necessary to further reduce the noise in the obtained back-EMFs. The traditional solution consists of placing a lowpass filter immediately after the switching function. However, the cutoff frequency of that filter has to be set quite low to obtain a clean enough signal, resulting in a large phase shift in the estimated back-EMFs. This introduces a delay in the estimation process and significantly degrades the performance of the estimator. An improvement was obtained in [27] by means of the so-called synchronous frequency tracking filter, and in [33] using a frequency-adaptive complex-coefficient filter (FACCF). Both filters basically behave as bandpass filters tuned on the estimated rotor speed produced by the PLL, which corresponds to the expected fundamental frequency of the back-EMFs. In this way, all the other frequency components of the estimated signal are filtered out without introducing an additional phase delay. The principle of operation of the FACCF is now explained as an example. Its behavior is given by the transfer function in (22)

$$\hat{e}_\alpha + j\hat{e}_\beta = \frac{\omega_c}{s - j\hat{\omega} + \omega_c}(z_\alpha + jz_\beta) \tag{22}$$

where j is the imaginary unit and ω_c is the cutoff frequency, which can be set equal to $2\hat{\omega}$. The resulting Bode diagram of the filter is shown in Figure 8.

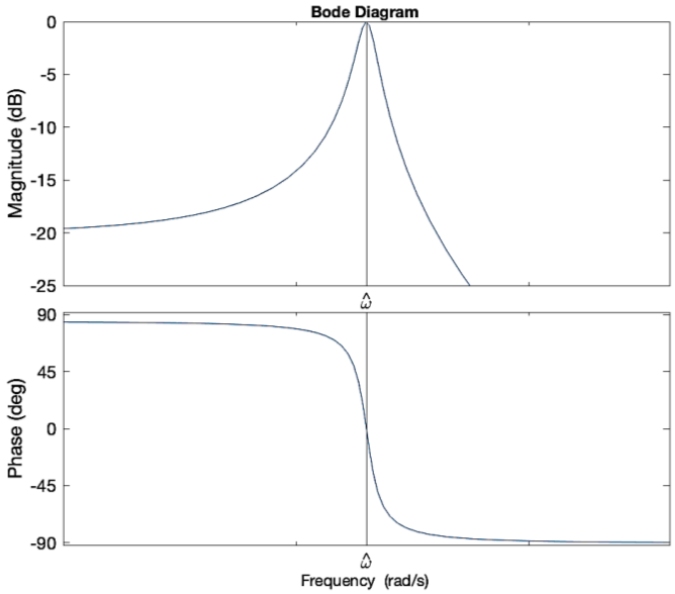

Figure 8. Magnitude and phase Bode diagram of the FACCF.

As can be seen from the plot, the FACCF behaves similarly to a bandpass filter tuned on the estimated rotor speed $\hat{\omega}$. At the corresponding frequency, a phase delay of zero is introduced, a condition that can improve the performance of the resulting SMO. Experimental tests carried out in [33] show that the FACCF has a good filtering effect on the estimated back-EMFs and demonstrate better performance of the algorithm with respect to the conventional SMO, both in steady state conditions and during transients such as acceleration/deceleration and load disturbances.

4. Rotor Flux Observer-Based Sensorless Algorithms

It is generally assumed that the performance of back-EMF-based algorithms deteriorates approaching the low-speed region [41,42]. This can be well explained by the fact that in that operating condition the amplitude of the motor back-EMFs is small and it is very difficult to obtain a sufficient signal-to-noise ratio to estimate the rotor position correctly. Moreover, back-EMF estimation becomes more sensitive to parameter uncertainties at low speeds. The effect of this drawback can be reduced using an RFO-based sensorless algorithm, which not only guarantees a better performance at low speeds but shows a good estimation accuracy and stability in the nominal speed range as well. The most common approach is to estimate the rotor flux components in the stationary reference frame. In this way, the rotor angle can be simply obtained by means of the arctan function. Three RFO algorithms chosen from the most promising ones in the technical literature are presented in this section. A nonlinear RFO introduced by Ortega et al. in [42] is considered first. The second algorithm examined is an adaptive RFO developed by Choi et al. in [45] to achieve a great robustness against dc bias errors and flux linkage constant uncertainty. Finally, a regression RFO presented in [50,51], based on a linear regression form, is analyzed.

4.1. Nonlinear RFO

This algorithm was developed in [42] for SPMSMs (it is therefore assumed that $L_d = L_q = L_s$). The starting point for the derivation of this position observer is consti-

tuted by the electrical equations expressed in the stationary reference frame α-β (2), (3), which can be rearranged as follows in (23)

$$L_s p\boldsymbol{i}_{\boldsymbol{\alpha\beta}} = -R_s\boldsymbol{i}_{\boldsymbol{\alpha\beta}} + \omega\varphi_m\begin{bmatrix}\sin\theta\\ -\cos\theta\end{bmatrix} + \boldsymbol{v}_{\boldsymbol{\alpha\beta}} \tag{23}$$

where $\boldsymbol{v}_{\boldsymbol{\alpha\beta}} = [v_\alpha,\ v_\beta]^T$ and $\boldsymbol{i}_{\boldsymbol{\alpha\beta}} = [i_\alpha,\ i_\beta]^T$. A new state variable $\boldsymbol{x}$ can be defined as in (24)

$$\boldsymbol{x} = L_s\boldsymbol{i}_{\boldsymbol{\alpha\beta}} + \varphi_m\begin{bmatrix}\cos\theta\\ \sin\theta\end{bmatrix} \tag{24}$$

Then a vector function η: $\mathbb{R}^2 \to \mathbb{R}^2$ is defined as in (25)

$$\eta(\boldsymbol{x}) = \boldsymbol{x} - L_s\boldsymbol{i}_{\boldsymbol{\alpha\beta}} \tag{25}$$

If the estimated state was exactly equal to the real one, the Euclidean norm of η would satisfy the condition in (26)

$$\|\eta(\boldsymbol{x})\|^2 = {\varphi_m}^2 \tag{26}$$

Since this is obviously not possible, because the state is unknown, an estimation error can be defined as in (27)

$$\varepsilon_{\hat{x}} = {\varphi_m}^2 - \|\eta(\hat{\boldsymbol{x}})\|^2 \tag{27}$$

Note that the error thus defined represents the squared distance between η and a circle of radius φ_m. The operating principle of this algorithm is based on the minimization of that error using the gradient search method, which can be implemented with Equation (28)

$$p\hat{\boldsymbol{x}} = \boldsymbol{v}_{\boldsymbol{\alpha\beta}} - R_s\boldsymbol{i}_{\boldsymbol{\alpha\beta}} - \frac{1}{2}\frac{\gamma}{4}\nabla_{\hat{x}}\left({\varepsilon_{\hat{x}}}^2\right) \tag{28}$$

where $\nabla_{\hat{x}}\left({\varepsilon_{\hat{x}}}^2\right)$ is the gradient of the squared estimation error calculated with respect to $\hat{\boldsymbol{x}}$, and γ is a gain parameter. At each calculation step, the derivative of the estimated state is updated so that $\varepsilon_{\hat{x}}$ is minimized. The resulting estimator is described by Equation (29)

$$p\hat{\boldsymbol{x}} = \boldsymbol{v}_{\boldsymbol{\alpha\beta}} - R_s\boldsymbol{i}_{\boldsymbol{\alpha\beta}} + \frac{\gamma}{2}\,\eta(\hat{\boldsymbol{x}})\left[{\varphi_m}^2 - \|\eta(\hat{\boldsymbol{x}})\|^2\right] \tag{29}$$

Finally, the rotor position can be derived from the estimated state as in (30)

$$\hat{\theta} = \tan^{-1}\left(\frac{\hat{x}_\beta - L_s i_\beta}{\hat{x}_\alpha - L_s i_\alpha}\right) \tag{30}$$

The position observer thus obtained has the advantage of being particularly easy to tune since it has only a gain parameter γ. Its validity has been demonstrated in [43], showing its ability to keep a low position estimation error during the tests, including speed and load steps, and speed reversal. However, the main drawback is that the precise value of the flux linkage constant of the motor is needed, making it susceptible to a possible parameter mismatch.

4.2. Adaptive RFO

This algorithm [45], developed for SPMSMs, represents the evolution of another flux observer that was introduced originally by Bobtsov et al. in [44]. In particular, a feedback loop was added with the aim to reduce the influence of parametric uncertainties on its performance, making it much more robust than the original one. First, the original observer is described in this paragraph, then the feedback compensation network is added. In the

derivation of this algorithm, the state to be observed consists directly of the components of the flux expressed in the stationary reference frame and it is defined as in (31)

$$\boldsymbol{x} = \varphi_m \begin{bmatrix} \cos\hat{\theta} \\ \sin\hat{\theta} \end{bmatrix} \tag{31}$$

Its dynamic equation can be derived from (2), (3) as in (32)

$$p\boldsymbol{x} = \boldsymbol{v}_{\boldsymbol{\alpha\beta}} - R_s \boldsymbol{i}_{\boldsymbol{\alpha\beta}} - L_s p \boldsymbol{i}_{\boldsymbol{\alpha\beta}} = \omega\varphi_m \begin{bmatrix} -\sin\theta \\ \cos\theta \end{bmatrix} \tag{32}$$

Theoretically, the state could be obtained by simply integrating the previous equation. However, this would lead to unacceptable estimation errors mainly due to the unknown initial conditions and to dc bias errors, which would cause the estimated state to diverge. Thus, it is necessary to define a state vector similar to the previous one, but whose initial condition is assumed equal to zero, as in (33)

$$p\boldsymbol{q} = \boldsymbol{v}_{\boldsymbol{\alpha\beta}} - R_s \boldsymbol{i}_{\boldsymbol{\alpha\beta}} - L_s p \boldsymbol{i}_{\boldsymbol{\alpha\beta}} \ , \ \boldsymbol{q}(0) = \begin{bmatrix} 0 \\ 0 \end{bmatrix} \tag{33}$$

Calling $\boldsymbol{\zeta}$ the initial condition of $\boldsymbol{x}$, Equation (34) can be derived

$$\boldsymbol{x} = \boldsymbol{q} + \boldsymbol{\zeta} \tag{34}$$

Taking into account (31) and (34), Equation (35) can be written

$$-\|\boldsymbol{q}\|^2 = 2\boldsymbol{q}^T\boldsymbol{\zeta} + \|\boldsymbol{\zeta}\|^2 - {\varphi_m}^2 \tag{35}$$

Note that equation (35) contains two constant terms, one of which ($\|\boldsymbol{\zeta}\|^2$) is unknown, while the other (${\varphi_m}^2$) is known but with possible uncertainties. To eliminate the effect of these terms, a highpass filter of equation $\frac{\alpha p}{p+\alpha}$ can be applied to both sides, obtaining two new variables as defined in (36), (37)

$$y(\boldsymbol{q}) = -\frac{\alpha p}{p+\alpha}\left(\|\boldsymbol{q}\|^2\right) \tag{36}$$

$$\boldsymbol{\Omega}(\boldsymbol{q}) = \frac{2\alpha p}{p+\alpha}(\boldsymbol{q}) \tag{37}$$

which are linked by Equation (38)

$$y(\boldsymbol{q}) \approx \ \boldsymbol{\Omega}(\boldsymbol{q})^T\boldsymbol{\zeta} \tag{38}$$

Note that the parameter α affects the bandwidth of the highpass filter. Equation (38) represents a form of linear regression with the unknown parameter $\boldsymbol{\zeta}$, which can be estimated by applying the gradient search algorithm, in a similar way to what happens for the nonlinear RFO previously described. The gradient method is implemented so that the quantity $\left(y(\boldsymbol{q}) - \boldsymbol{\Omega}(\boldsymbol{q})^T\boldsymbol{\zeta}\right)^2$ is minimized, as in (39)

$$p\hat{\boldsymbol{\zeta}} = \boldsymbol{\Gamma}\boldsymbol{\Omega}(\boldsymbol{q})\left(y(\boldsymbol{q}) - \boldsymbol{\Omega}(\boldsymbol{q})^T\hat{\boldsymbol{\zeta}}\right) \tag{39}$$

where $\boldsymbol{\Gamma}$ is a gain parameter. Finally, the estimated rotor position can be obtained as in (40)

$$\hat{\theta} = \tan^{-1}\left(\frac{\hat{x}_\beta}{\hat{x}_\alpha}\right) \tag{40}$$

For better understanding, Bobtsov's observer is schematized in Figure 9.

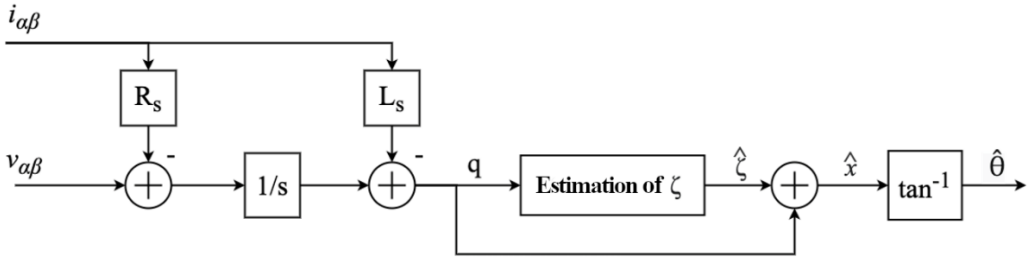

Figure 9. Bobtsov's position observer.

Note that the algorithm thus obtained solves the problem related to the unknown initial conditions, but it can still be affected by dc bias errors. Indeed, if the quantities that are integrated have a dc bias, this causes the estimated state to diverge. For this reason, a feedback compensation network has been added by Choi et al. [45]. It is based on the consideration that the initial estimated flux $\hat{\zeta}$ must have a magnitude equal to φ_m. If this does not happen, an error in the estimation of ζ can be defined as in (41)

$$\varepsilon_{\hat{\zeta}} = \|\hat{\zeta}\|^2 - {\varphi_m}^2 \tag{41}$$

In order to minimize this error, the gradient algorithm can be applied a second time, obtaining a compensating term that can be added before the integrator. Calling $\hat{\boldsymbol{q}}$ the compensated value of state $\boldsymbol{q}$, the resulting updating equation for $\hat{\boldsymbol{q}}$ is reported in (42).

The adaptive RFO-based position estimator thus obtained is summarized in (43), while its operating diagram is shown in Figure 10.

$$p\hat{\boldsymbol{q}} = \boldsymbol{v}_{\boldsymbol{\alpha\beta}} - R_s\boldsymbol{i}_{\boldsymbol{\alpha\beta}} - L_s p\boldsymbol{i}_{\boldsymbol{\alpha\beta}} + \boldsymbol{\Gamma}_1\hat{\zeta}\left(\|\hat{\zeta}\|^2 - {\varphi_m}^2\right) \tag{42}$$

$$\begin{cases} \dot{\hat{\boldsymbol{q}}} = \boldsymbol{v}_{\boldsymbol{\alpha\beta}} - R_s\boldsymbol{i}_{\boldsymbol{\alpha\beta}} - L_s p\boldsymbol{i}_{\boldsymbol{\alpha\beta}} + \boldsymbol{\Gamma}_1\hat{\zeta}\left(\|\hat{\zeta}\|^2 - {\varphi_m}^2\right) \\ \hat{\boldsymbol{q}}(0) = [0,\ 0]^T \\ \dot{\hat{\zeta}} = \boldsymbol{\Gamma}_2\boldsymbol{\Omega}(\hat{q})\left(y(\hat{\boldsymbol{q}}) - \boldsymbol{\Omega}(\hat{\boldsymbol{q}})^T\hat{\zeta}\right),\ \hat{\zeta}(0) \in \mathbb{R}^2 \\ y(\hat{\boldsymbol{q}}) = \frac{-\alpha p}{p+\alpha}\|\hat{\boldsymbol{q}}\|^2,\ y(0) = 0 \\ \boldsymbol{\Omega}(\hat{\boldsymbol{q}}) = \frac{\alpha p}{p+\alpha}2\hat{\boldsymbol{q}},\ \boldsymbol{\Omega}(0) = [0,\ 0]^T \\ \hat{\boldsymbol{x}} = \hat{\boldsymbol{q}} + \hat{\zeta} \\ \hat{\theta} = \tan^{-1}\left(\frac{\hat{x}_\beta}{\hat{x}_\alpha}\right) \end{cases} \tag{43}$$

Experimental tests are also shown in [45], in which the performance of the algorithm was evaluated during no-load starting, full load steps at various speed levels and speed reversal. Only a full load step at low speed caused the stability to collapse, but that did not happen in the case of a load ramp. Moreover, a comparison between Bobtsov's observer and the adaptive RFO was carried out by the authors, introducing some mismatches in the motor parameters including the flux linkage constant. While the position estimation degraded significantly in the case of Bobtsov's observer, the adaptive RFO was able to compensate them maintaining a sufficiently low estimation error. Moreover, an intentional voltage dc bias was added to the output of the current controller in the plant. The pure integration present in Bobtsov's observer made the estimation error diverge, while the compensation feedback introduced in the adaptive RFO avoided this phenomenon.

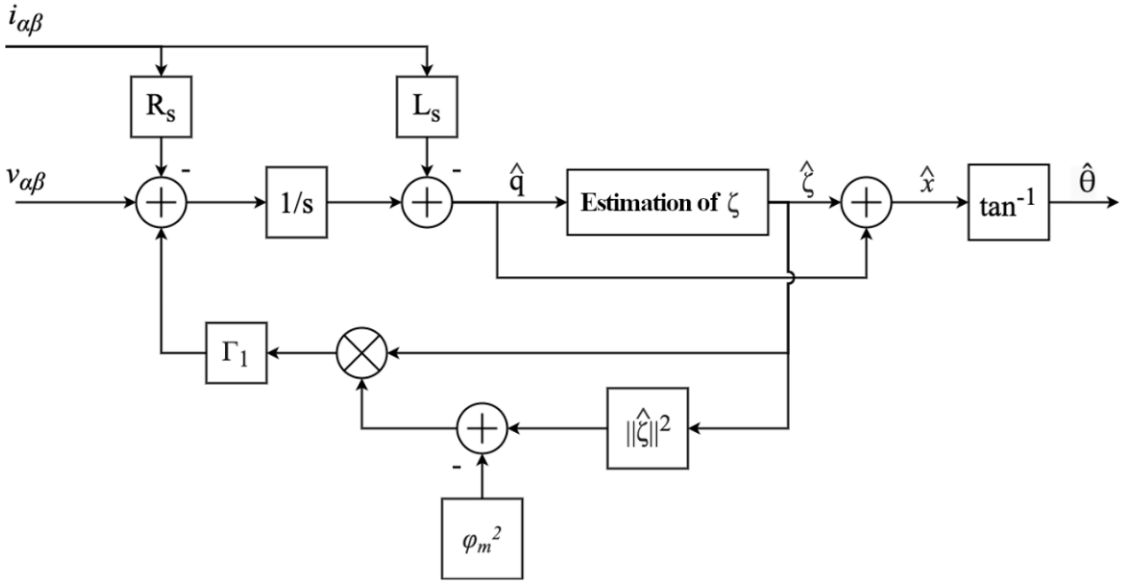

Figure 10. Scheme of the adaptive RFO sensorless algorithm.

4.3. Regression RFO

The regression RFO was introduced by Choi et al. in [50,51] as an extension of the previous algorithm to the case of IPMSMs. However, the operating principle of the resulting RFO is slightly different from the previous one, and, as the authors themselves state, it can be adapted for use with SPMSMs. Since the derivation of the regression RFO algorithm is quite complex, only the main steps are shown below. The starting point is the definition of the stator flux $\boldsymbol{\lambda}$ as in (44), whose dynamic equation can be expressed as in (45)

$$\boldsymbol{\lambda} = \begin{bmatrix} L_s + \frac{\Delta L}{2}\cos 2\theta & \frac{\Delta L}{2}\sin 2\theta \\ \frac{\Delta L}{2}\sin 2\theta & L_s - \frac{\Delta L}{2}\cos 2\theta \end{bmatrix} \begin{bmatrix} i_\alpha \\ i_\beta \end{bmatrix} + \varphi_m \begin{bmatrix} \cos\theta \\ \sin\theta \end{bmatrix} \tag{44}$$

$$p\boldsymbol{\lambda} = \boldsymbol{v}_{\boldsymbol{\alpha\beta}} - R_s \boldsymbol{i}_{\boldsymbol{\alpha\beta}} \tag{45}$$

After a few mathematical passages, a different expression for $\boldsymbol{\lambda}$ can be obtained as in (46)

$$\boldsymbol{\lambda} = L_q \boldsymbol{i}_{\boldsymbol{\alpha\beta}} + \left(\Delta L \boldsymbol{i}_{\boldsymbol{\alpha\beta}}{}^T \begin{bmatrix} \cos\theta \\ \sin\theta \end{bmatrix} + \varphi_m \right) \begin{bmatrix} \cos\theta \\ \sin\theta \end{bmatrix} \tag{46}$$

Then, the state $\boldsymbol{x}$ to be observed, called "active flux", is defined as in (47)

$$\boldsymbol{x} = \boldsymbol{\lambda} - L_q \boldsymbol{i}_{\boldsymbol{\alpha\beta}} = \left(\Delta L \boldsymbol{i}_{\boldsymbol{\alpha\beta}}{}^T \begin{bmatrix} \cos\theta \\ \sin\theta \end{bmatrix} + \varphi_m \right) \begin{bmatrix} \cos\theta \\ \sin\theta \end{bmatrix} \tag{47}$$

It should be noted that, in the case of SPMSMs, $\Delta L = 0$ and the active flux coincides with the rotor flux defined in previous algorithms. Additionally, in this case, the rotor position can be obtained from the active flux by means of the arctan function as in (40). To estimate $\boldsymbol{x}$, a new linear regression form is derived, eliminating the effect of unknown constant terms thanks to the appliance of a highpass filter of equation $\frac{\alpha p}{p+\alpha}$, identical to the

one previously used in the adaptive RFO. Then, the gradient search algorithm is applied to the linear regression form to obtain the position observer summarized in (48)

$$\begin{cases} p\hat{\boldsymbol{\lambda}} = \boldsymbol{v}_{\boldsymbol{\alpha\beta}} - R_s\boldsymbol{i}_{\boldsymbol{\alpha\beta}} + \gamma\boldsymbol{\Omega}_2\left(y - \boldsymbol{\Omega}_2{}^T\hat{\boldsymbol{x}}\right),\ \hat{\boldsymbol{\lambda}}(0) = \varphi_m\begin{bmatrix}\cos\theta(0)\\ \sin\theta(0)\end{bmatrix} \\ \hat{\boldsymbol{x}} = \hat{\boldsymbol{\lambda}} - L_q\boldsymbol{i}_{\boldsymbol{\alpha\beta}} \\ \boldsymbol{\Omega}_1 = \frac{\alpha}{p+\alpha}\left(\boldsymbol{v}_{\boldsymbol{\alpha\beta}} - R_s\boldsymbol{i}_{\boldsymbol{\alpha\beta}} + \alpha L_q\boldsymbol{i}_{\boldsymbol{\alpha\beta}}\right) - \alpha L_q\boldsymbol{i}_{\boldsymbol{\alpha\beta}} \\ \boldsymbol{\Omega}_2 = \frac{\alpha}{p+\alpha}\left(\boldsymbol{v}_{\boldsymbol{\alpha\beta}} - R_s\boldsymbol{i}_{\boldsymbol{\alpha\beta}} + \alpha L_d\boldsymbol{i}_{\boldsymbol{\alpha\beta}}\right) - \alpha L_d\boldsymbol{i}_{\boldsymbol{\alpha\beta}} \\ y = \frac{1}{p+\alpha}\boldsymbol{\Omega}_1{}^T\boldsymbol{\Omega}_2 + \frac{1}{2}\left(\frac{1}{\alpha} - \frac{1}{p+\alpha}\right)\|\boldsymbol{\Omega}_1\|^2 + \Delta L\boldsymbol{\Omega}_1{}^T\left(\frac{\alpha}{p+\alpha}\boldsymbol{i}_{\boldsymbol{\alpha\beta}}\right) \\ \hat{\theta} = \tan^{-1}\left(\frac{\hat{x}_\beta}{\hat{x}_\alpha}\right) \end{cases} \tag{48}$$

where γ is a gain parameter. The operating scheme of the regression RFO is shown in Figure 11.

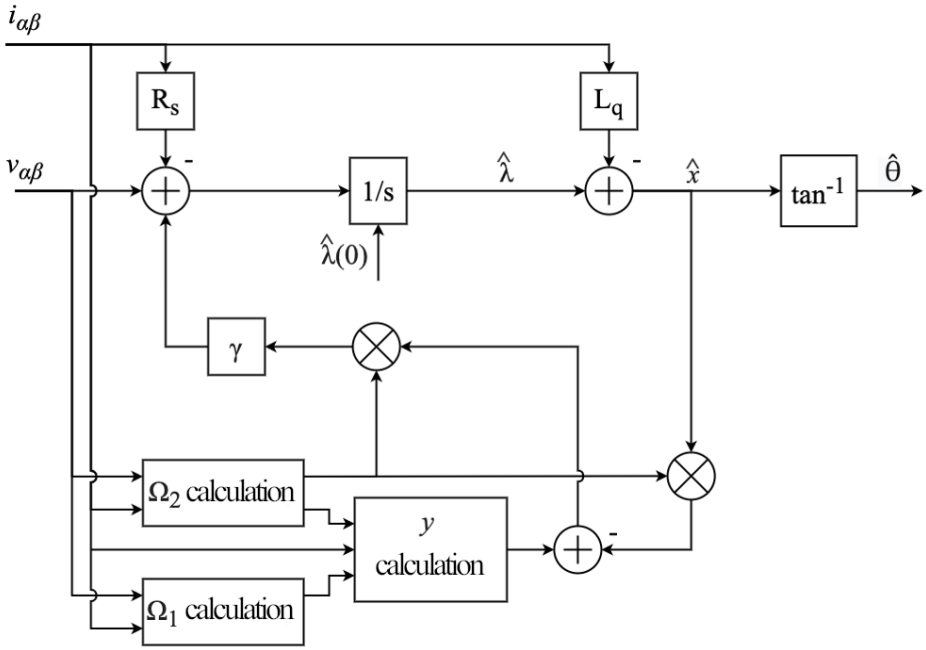

Figure 11. Scheme of the regression RFO sensorless algorithm.

In the case of SPMSMs, the equations can be simplified as follows in (49)

$$\begin{cases} p\hat{\boldsymbol{\lambda}} = \boldsymbol{v}_{\boldsymbol{\alpha\beta}} - R_s\boldsymbol{i}_{\boldsymbol{\alpha\beta}} + \gamma\boldsymbol{\Omega}\left(y - \boldsymbol{\Omega}^T\hat{\boldsymbol{x}}\right),\ \hat{\boldsymbol{\lambda}}(0) = \varphi_m\begin{bmatrix}\cos\theta(0)\\ \sin\theta(0)\end{bmatrix} \\ \hat{\boldsymbol{x}} = \hat{\boldsymbol{\lambda}} - L_s\boldsymbol{i}_{\boldsymbol{\alpha\beta}} \\ \boldsymbol{\Omega} = \frac{\alpha}{p+\alpha}\left(\boldsymbol{v}_{\boldsymbol{\alpha\beta}} - R_s\boldsymbol{i}_{\boldsymbol{\alpha\beta}} + \alpha L_s\boldsymbol{i}_{\boldsymbol{\alpha\beta}}\right) - \alpha L_s\boldsymbol{i}_{\boldsymbol{\alpha\beta}} \\ y = \frac{1}{2}\left(\frac{1}{\alpha} + \frac{1}{p+\alpha}\right)\|\boldsymbol{\Omega}\|^2 \\ \hat{\theta} = \tan^{-1}\left(\frac{\hat{x}_\beta}{\hat{x}_\alpha}\right) \end{cases} \tag{49}$$

Note that, unlike the previous RFO algorithms, the flux linkage constant does not appear in the dynamic equations of the state, but it is only used to compute the initial value of $\boldsymbol{\lambda}$. This can make the algorithm particularly robust against uncertainties in the value of φ_m. Another advantage of the regression RFO is that the tuning process involves only one gain parameter. However, as explained by the authors, the stability and the response time of the observer are at maximum when that gain is not equal to a fixed value, but a

speed-dependent gain is adopted. For this reason, a law to obtain the correct gain as a function of the rotor speed has to be introduced in the scheme, and this may complicate the implementation of the algorithm. The experimental results shown in [50] demonstrate a good convergence of the estimated position during all tests, also when an intentional 20% error was introduced in the flux linkage constant value. Moreover, the observer's performance was also good at low speed as it was able to withstand a nominal torque step.

5. Comparison of Different Sensorless Algorithms in the Low-Speed Region on a Test Bench with an SPMSM

As can be deduced from the previous sections, a very large number of passive sensorless algorithms for PMSMs have been presented and analyzed in the technical literature. This makes it difficult to evaluate which is the most suitable position observer in the absolute sense for the realization of a sensorless control system, as they all have different characteristics and their effectiveness depends on what is required by the single application. Moreover, each work published that includes experimental tests shows results obtained on a different bench for what concerns the power of the drive, the motor characteristics, the switching frequency and the operating speed range. Despite this, it is possible to identify some criteria by which different algorithms can be compared, such as:

- The ease of implementation and computational complexity required for the operation. This can be a critical aspect since some algorithms characterized by a particularly low estimation error may require an intensive computational effort and could increase the overall cost and operating stability of the system. The choice of the most suitable algorithm in this sense should be made taking into account the precision required in estimating the position and the computational resources available.
- The complexity of the tuning process, for what concerns observer gains, cutoff frequency of filters and other parameters. Some applications may expect the algorithm to be used in conditions that are always the same, requiring only one preliminary calibration of the operating parameters. Instead, other applications may require the tuning process to be particularly easy and fast as it may be carried out by the customer depending on the specific purpose.
- The operating speed range. Some applications require the algorithm to be effective in a wide speed range, e.g., from standstill to the nominal speed, while in some other cases the motor is expected to operate at a fixed speed. This aspect can be particularly critical when approaching the low-speed region.
- The type of load. The stability and the dynamic response of a sensorless algorithm often depends on how the load is applied to the motor. For example, some applications such as compressors, ventilation systems or transports usually have a speed-dependent load, while in some cases the system must be able to withstand sudden load steps.
- The robustness against parameter variations. In most cases, the algorithm requires the knowledge of some motor parameters to operate correctly, such as the stator resistance and inductance or the flux linkage constants. These parameters are often not known with sufficient precision and can also change during the operation (e.g., the stator resistance can vary with temperature). For some applications, the system is required to maintain a low estimation error even in the presence of strong variations or mismatches of the motor parameters.

As explained in previous sections, the performance of a passive sensorless algorithm generally degrades in the low-speed operating region. For this reason, the generally adopted approach consists of using a combination of an active algorithm (based on high-frequency signal injection) and a passive one. The active method can be used for starting the motor from standstill and obtain the estimated rotor position during low-speed operation. Then, when the speed is above a certain threshold, a transition to a passive algorithm can be performed. This allows the well-known drawbacks associated with active signal injection, such as current distortion, additional losses and acoustic noise, to be limited. A highly desirable evolution of this strategy is the adoption of a single passive algorithm for the entire

speed range, as this would eliminate the signal injection completely and greatly simplify the implementation of the control system. In order to reduce or possibly eliminate the use of active algorithms, the essential condition is that the adopted passive algorithm works with sufficient precision in the widest possible speed range. For this reason, its performance at lower speeds becomes critical to realize a full-range sensorless control system.

In [54], an experimental comparison among five different passive algorithms was carried out on an SPMSM. The algorithms were chosen from among the most promising ones found in the literature and they were implemented on the same test bench in order to achieve a fair comparison. The study focused on their performances at low speed (i.e., under 20% of the motor's rated speed) and the test conditions were the same for all, recreating the characteristics of a drive for typical industrial applications. The main results obtained in this work are reviewed here, as they give an idea on how the different types of passive algorithms described in the previous sections would perform in that situation. The list of algorithms, which includes two back-EMF-based methods and three rotor flux observers, is as follows:

- The "Enhanced Linear Active Disturbance Rejection Controller" (ELADRC), a method based on direct back-EMF estimation by means of LESOs, described in [21].
- A sliding-mode back-EMF observer with the adoption of the frequency adaptive filter, the "FACCF-SMO" described in [33].
- The nonlinear RFO described in [42].
- The adaptive RFO (evolution of the original Bobtsov's observer) described in [45].
- The regression RFO described in [50].

All of the algorithms were implemented on the same FOC scheme and the same tests were carried out for each, including speed steps, load steps and full load starting. Moreover, their robustness against a mismatch introduced in the stator inductance value was tested and compared. The test bench consisted of a dSpace Microlab Box control platform on which all the algorithms were implemented, a PWM inverter (DC link voltage: 550 V) and an SPMSM, whose parameters are listed in Table 1. Another SPMSM (rated torque: 27 Nm) was coupled with the motor under test and controlled by a dedicated system to generate the load torque, as shown in Figure 12. The PWM frequency was 5 kHz and the deadtime of 4 µs was not compensated. An incremental encoder (resolution: 0.1°) was used to measure the rotor angle, only for comparison with the estimated one.

Table 1. Parameters of the SPMSM on which the algorithms were tested.

Parameter	Value
Rated output power	1000 W
Number of poles	8
Rated speed	520 rad/s
Rated voltage	376 V
Maximum current	2.21 A
Rated torque	2 Nm
Stator resistance R_s	1.6 Ω
Stator inductance L_s	5.7 mH
Flux constant φ_m	0.147 Wb

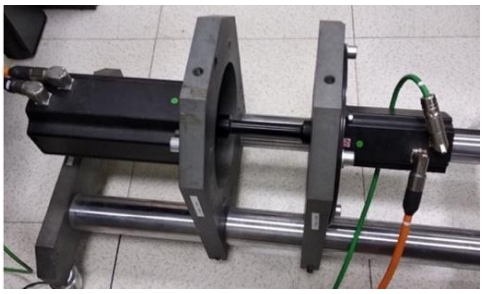

Figure 12. SPMSM under test (motor on the right) and SPMSM used to generate the load torque (motor on the left).

5.1. Performance of the Algorithms during Speed Steps

Starting from standstill with no load, three consecutive steps were applied to the reference speed. First it was set to 3% of the rated speed, then to 10% and finally to 20%. At that point, a rated load step was applied. Figure 13 shows the rotor speed (reference, estimated and measured) and the estimation error of the rotor position with respect to the measured one. Moreover, a zoom on the estimated and measured rotor angle is shown when the speed was increased from 3% to 10% of the rated value. The values of position estimation error during the whole test and the starting time are summarized in Table 2.

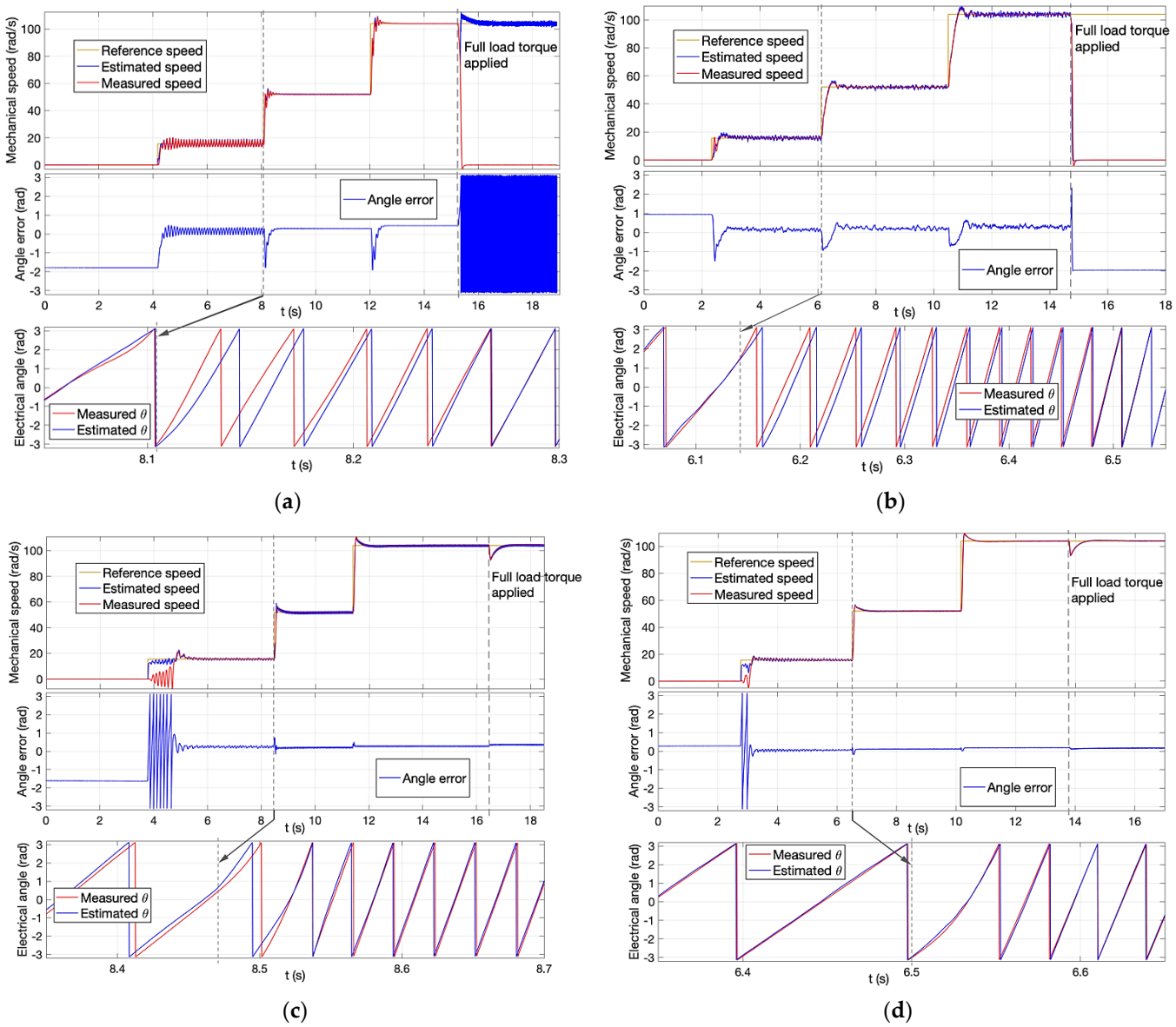

Figure 13. *Cont.*

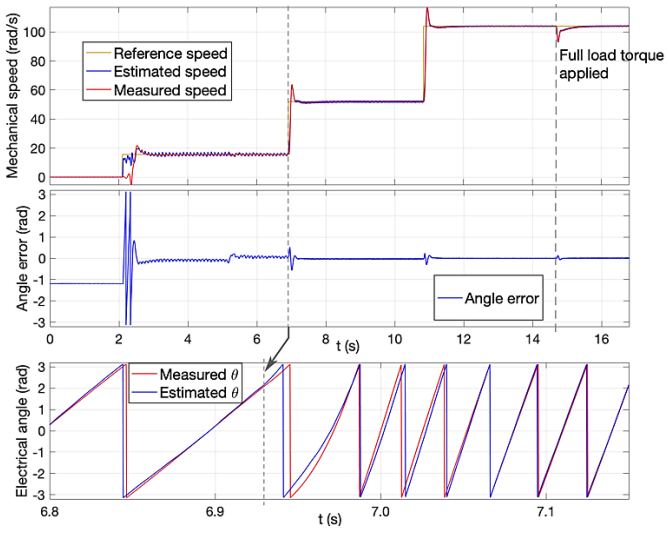

(**e**)

Figure 13. Speed, estimated angle error and zoom on measured/estimated angle when 3–10–20% speed steps are applied, and a full load step is applied at 20% of rated speed: (**a**) ELADRC algorithm; (**b**) FACCF-SMO algorithm; (**c**) nonlinear RFO; (**d**) adaptive RFO; (**e**) regression RFO.

Table 2. Position estimation error after appliance of speed steps and load step, and starting time.

Algorithm	**Angle Estimation Error (rad) Mean Value/Ripple Amplitude**				**Starting Time 0–3% ω_N**
	3% ω_N	**10% ω_N**	**20% ω_N**	**Full Load Applied**	
ELADRC	0.15/0.4	0.28/0.03	0.45/0.02	Not successful	0.2 s
FACCF-SMO	0.15/0.3	0.2/0.3	0.3/0.25	Not successful	0.3 s
Nonlinear RFO	0.25/0.18	0.2/0.09	0.27/0.07	0.36/0.08	1.1 s
Adaptive RFO	0.05/0.14	0.12/0.04	0.18/0.04	0.16/0.05	0.4 s
Regression RFO	−0.1/0.12	−0.03/0.05	0.0/0.04	0.01/0.05	0.4 s

Results show that the two back-EMF-based algorithms had a generally higher estimation error at low speed, as expected, although their starting time was shorter. In particular, a wide oscillation can be observed in the angle estimated by the ELADRC at 3% of the rated speed. Moreover, these two algorithms could not withstand the appliance of a full load step at 20% of the rated speed. On the other hand, the three RFOs were able to follow the reference speed correctly also after the load step, maintaining an acceptable estimation error. The adaptive RFO and regression RFO showed a short starting time and the highest estimation accuracy. Another aspect should be noted observing the zoom on the estimated and real position. After the appliance of the second speed step, the convergence of the two back-EMF algorithms took longer than in the case of RFOs. This can be explained by the fact that the RFOs do not need the information about the rotor speed to observe the rotor position, while in the other case the speed is used in the estimation process (as it appears in the equations). Since the speed is provided by the PLL starting from the estimated position, this makes the dynamic response longer.

5.2. Performance of the Algorithms during Load Steps at 10% of Rated Speed

Load steps were applied at 10% of the rated speed, starting from the no-load condition. Only the adaptive RFO and the regression RFO could withstand a rated torque step, while in the other cases the load torque was applied in two consecutive steps (0–50–100%). However, even in this case, FACCF-SMO was not able to withstand the rated torque. Figure 14 shows

the rotor speed, the angle error and the stator current during the test. The values of the angle error are summarized in Table 3.

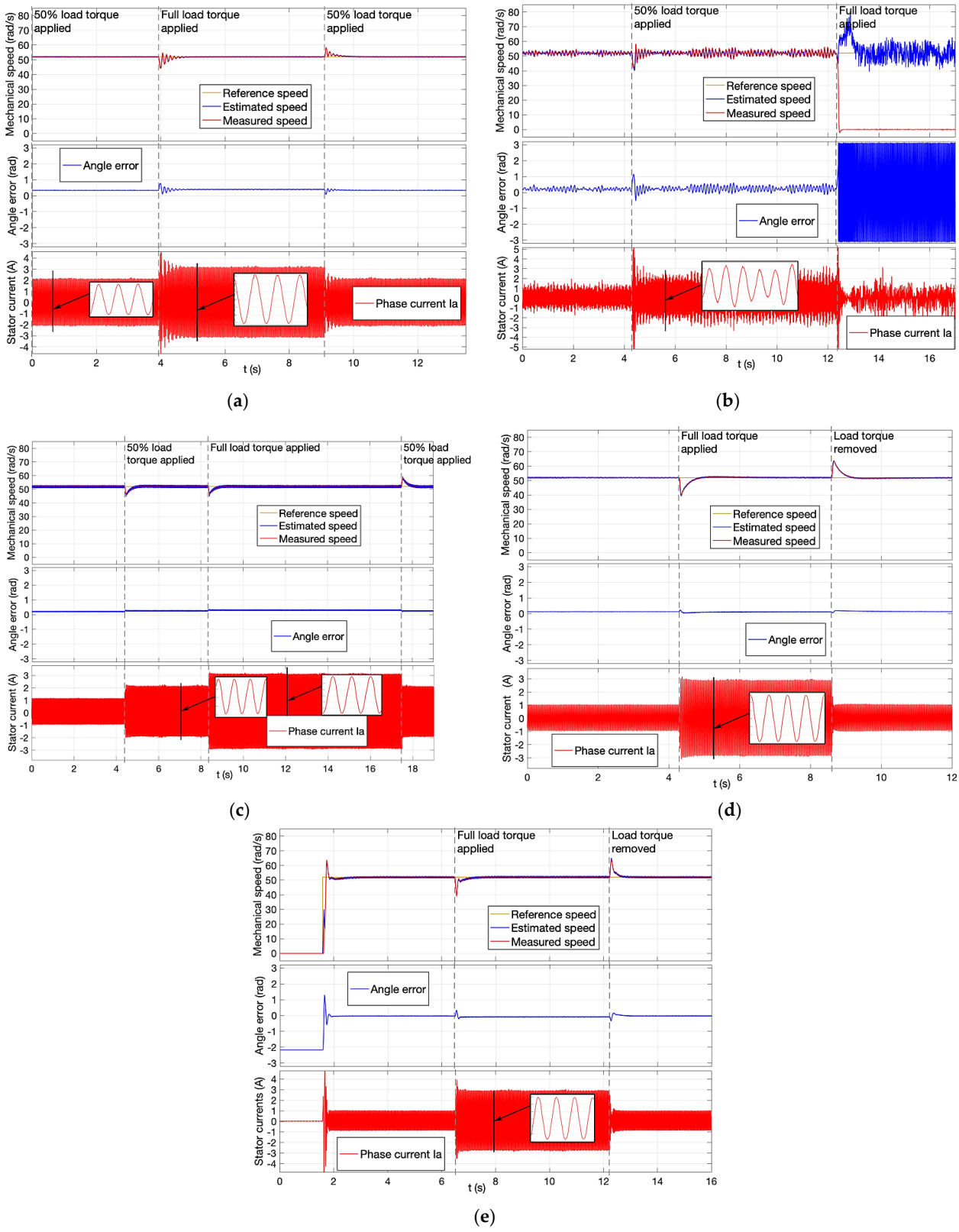

Figure 14. Speed, estimated angle error and stator current after the appliance of load torque steps: (**a**) ELADRC algorithm; (**b**) FACCF-SMO algorithm; (**c**) nonlinear RFO; (**d**) adaptive RFO; (**e**) regression RFO.

Table 3. Position estimation error after appliance of load steps at 10% of rated speed.

Algorithm	Angle Estimation Error (rad) Mean Value/Variation from the No-Load Condition	
	Half Load Applied	**Full Load Applied**
ELADRC	$0.33/\Delta\varepsilon_\theta = 0.05$	$0.39/\Delta\varepsilon_\theta = 0.11$
FACCF-SMO	$0.25/\Delta\varepsilon_\theta = 0.05$	Not successful
Nonlinear RFO	$0.25/\Delta\varepsilon_\theta = 0.05$	$0.3/\Delta\varepsilon_\theta = 0.1$
Adaptive RFO	N.A.	$0.12/\Delta\varepsilon_\theta = 0$
Regression RFO	N.A.	$-0.08/\Delta\varepsilon_\theta = -0.05$

Results show that the adaptive RFO and the regression RFO reacted well to the appliance of a full torque step, with a very low angle error variation with respect to the no-load condition. The nonlinear RFO and the ELADRC algorithm could manage the appliance of the full load in two gradual steps, while the FACCF-SMO lost stability when the load torque was set to its rated value.

5.3. Performance of the Algorithms during Full Load Starting

Starting from standstill, the rated load torque was applied and then the reference speed was set to 3% of its rated value. The results are shown in Figure 15.

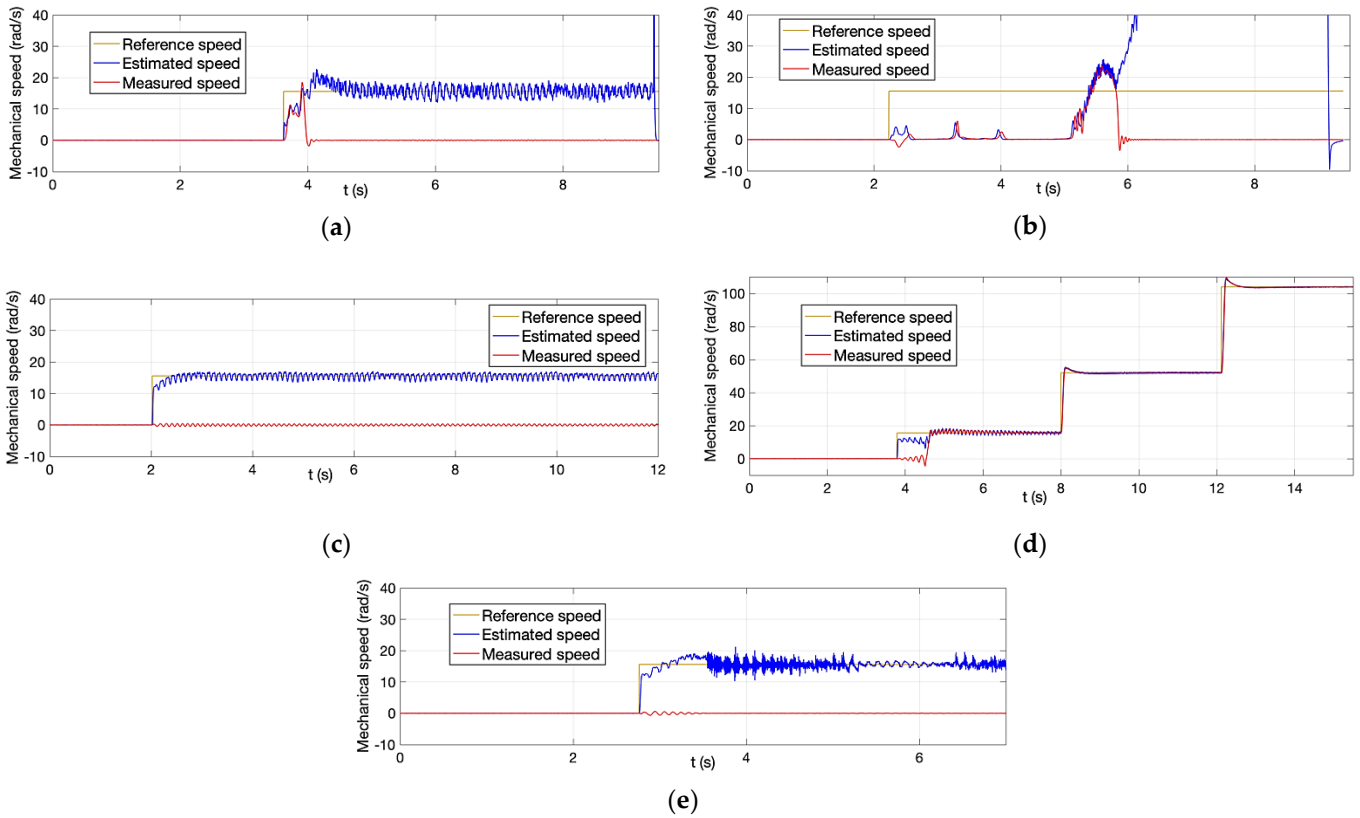

Figure 15. Reference, estimated and measured speed during starting with full load applied: (**a**) ELADRC algorithm; (**b**) FACCF-SMO algorithm; (**c**) nonlinear RFO; (**d**) adaptive RFO; (**e**) regression RFO.

As can be seen from the graphs, starting at full load was successful only with the adaptive RFO. Since the motor started in that case, the steps at 10% and 20% of the rated speed were also applied, obtaining a good response. The other algorithms were not able to start the motor correctly, resulting therefore in not being suitable for a full-range application in which a very low-speed operation at rated load torque is expected.

5.4. Robustness of the Algorithms against Inductance Variations

While keeping the reference speed equal to 10% of its rated value and applying the full load torque, mismatches in the stator inductance value given to the algorithms were introduced in order to test their robustness. Since the FACCF-SMO could not withstand the rated load torque at that speed, it was tested at half load. First L_s was changed from 5.7 mH (its real value) to 3 mH, then it was set to 5.7 mH again, and finally to 9 mH. The results are shown in Figure 16, while the values of the estimation error for each case are reported in Table 4.

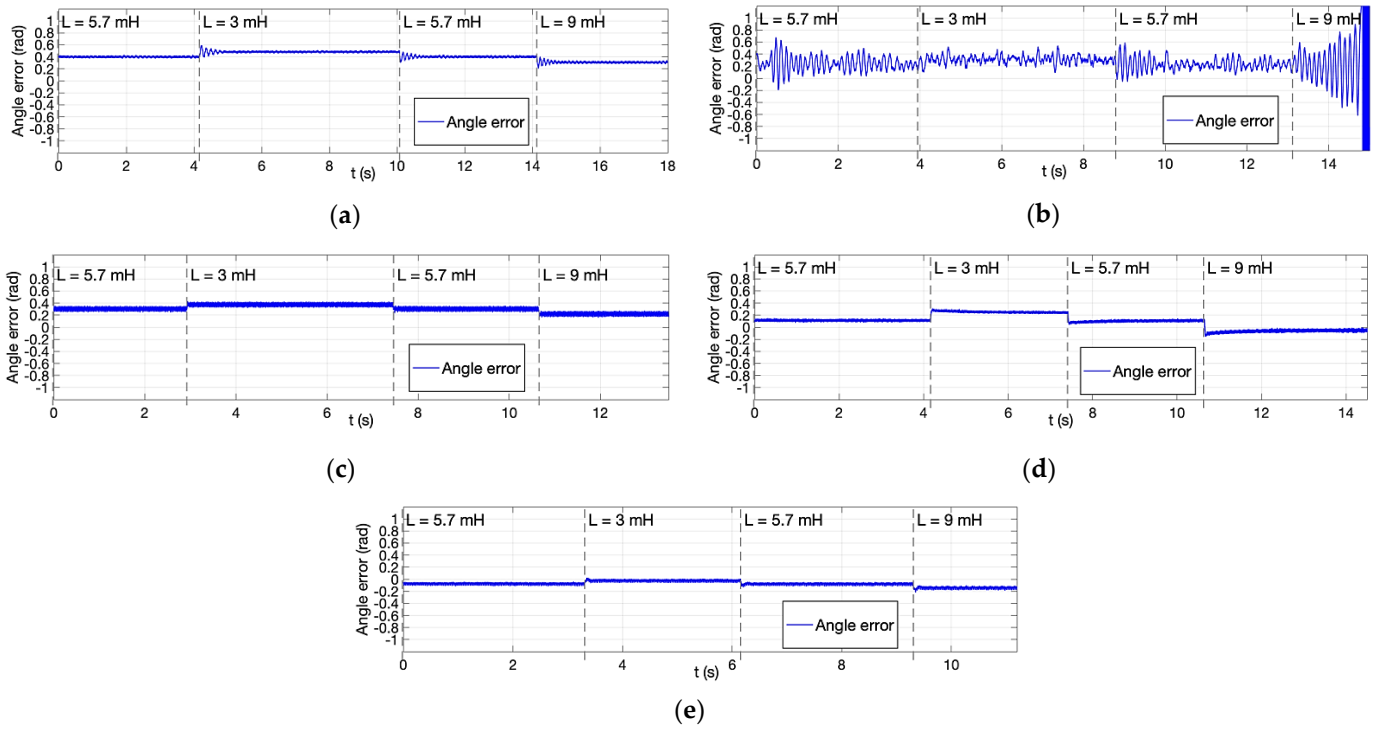

Figure 16. Position estimation error after introducing variations in the stator inductance value: (**a**) ELADRC algorithm; (**b**) FACCF-SMO algorithm; (**c**) nonlinear RFO; (**d**) adaptive RFO; (**e**) regression RFO.

Table 4. Position estimation error with mismatches in the value of L_s at 10% of rated speed.

Algorithm	**Angle Estimation Error (rad)** **Mean Value/Variation from the Real Inductance Condition**	
	L_s **= 3 mH**	L_s **= 9 mH**
ELADRC	$0.48/\Delta\varepsilon_\theta = 0.09$	$0.31/\Delta\varepsilon_\theta = -0.08$
FACCF-SMO	$0.3/\Delta\varepsilon_\theta = 0.05$	Unstable
Nonlinear RFO	$0.38/\Delta\varepsilon_\theta = 0.08$	$0.22/\Delta\varepsilon_\theta = -0.08$
Adaptive RFO	$0.25/\Delta\varepsilon_\theta = 0.13$	$-0.05/\Delta\varepsilon_\theta = -0.17$
Regression RFO	$-0.03/\Delta\varepsilon_\theta = 0.05$	$-0.15/\Delta\varepsilon_\theta = -0.07$

As can be deduced from the results, the regression RFO appears to be the most robust in the presence of a stator inductance value mismatch, as its estimation error varied by 0.05 rad, which corresponds to 2.9° when L_s was set to 3 mH and by 0.07 rad, which corresponds to 4.0°, when L_s was set to 9 mH. A slightly larger variation was observed with the nonlinear RFO and ELADRC, which could still maintain a variation of the error below $\pm$ 0.1 rad, which corresponds to 5.7°. The adaptive RFO showed a higher variation, but it was able to maintain a good stability during the test, while the FACCF-SMO became unstable when L_s was changed to 9 mH.

6. Conclusions

Sensorless control of PMSMs has become increasingly important in recent years to avoid the additional cost and reliability drawbacks associated with the use of a traditional position sensor in FOC schemes. Sensorless algorithms can mainly be divided into two types, active methods based on high-frequency signal injection and passive methods based on the estimation of back-EMFs or rotor flux. Although active methods work well over the entire speed range, they cause drawbacks (current distortion, losses, acoustic noise), which can be avoided using passive algorithms.

This paper proposed a review of the main types of passive sensorless algorithms, analyzing the different approaches proposed in the technical literature over the last few years. Two main families of passive methods were considered. The first one includes the so-called back-EMF-based algorithms, which derive the rotor position from an estimate of the back-electromotive forces of the motor using a PLL. As can be deduced from the experimental results presented in many works, the presence of the PLL in the estimation process generally deteriorates the dynamic response of the position estimator. Moreover, it is worth noting that back-EMF methods often require knowledge about the rotor speed to operate. Among these, algorithms based on linear disturbance observers and algorithms based on sliding mode were considered and analyzed in detail as they represent the most common approaches. For what concerns the sliding mode observers, a review of the most used switching functions was also presented. From various studies published in the literature, the sigmoid function and the super-twisting function appear to be the best ones in terms of harmonic content in the estimated signals. The second class of passive methods analyzed in this article is the one of the so-called rotor flux observers, which estimate the components of the rotor flux in the stationary or rotating reference frame and derive the rotor angle directly from them (usually by means of the arctan function). Their structure is often more complex, with respect to back-EMF methods, but they generally operate better at lower speeds since, in contrast to what happens to the back-EMFs, the rotor flux does not vanish at standstill. In addition, no knowledge about the rotor speed is required in the estimation process. Three types of RFOs were considered, chosen from among the most recent ones. The analysis included a nonlinear RFO, an adaptive RFO and a regression RFO. Their common feature is the use of the gradient search algorithm, which is implemented in different schemes. The nonlinear RFO can achieve a good estimation accuracy, but its performance can be affected by parameter mismatches, especially with regard to the flux linkage constant. The other two algorithms solve these problems as they implement feedback compensation networks to minimize the effect of uncertainties in the parameters and dc bias errors. Their validity has been demonstrated in many works published in the literature, testing them in various load conditions at different speeds. The low-speed performance of a sensorless algorithm is particularly important to limit as much as possible the use of active algorithms and their associated drawbacks. However, all the works considered, which are present in the technical literature, show experimental results obtained on different benches and in different test conditions, making it difficult to establish which is the most suitable one for a low-speed application. For that reason, an experimental comparison on an SPMSM operating at low speed has been reported, in which two back-EMF algorithms and three RFOs are implemented on the same test bench to achieve a fair comparison. The results show the superiority of RFOs over the back-EMF estimators in a speed range up to 20% of the rated value, especially with regard to the adaptive RFO, which was able to start the motor even with nominal torque applied.

From the analysis carried out, it can be concluded that the use of a sensorless algorithm can effectively replace the use of a position transducer for those applications where precise position control is not required, making it possible to reduce the cost of the drive and to increase its reliability. The field of application of passive sensorless algorithms includes drives for traction, industrial plants and household appliances, for which many of the algorithms presented are already widespread. From the results obtained, it can be deduced that, in cases where the motor has to operate in a speed range close to the nominal one,

the back-EMF algorithms such as SMOs could be preferred by virtue of their simplicity of implementation. On the other hand, in applications where low speed operation is also required, the algorithms based on RFOs guarantee greater estimation accuracy and more stable performance, even making it possible to start the motor at full load in some cases without the aid of high-frequency injection techniques.

Author Contributions: Conceptualization, M.M., M.P. and L.V.; data curation, A.B., L.C., S.C. and K.K.; formal analysis, A.B.; investigation, A.B., L.C., S.C. and K.K.; supervision, M.M., M.P. and L.V.; validation, A.B.; writing—original draft, A.B.; writing—review and editing, M.M., M.P. and L.V. All authors have read and agreed to the published version of the manuscript.

Funding: This research received no external funding.

Conflicts of Interest: The authors declare no conflict of interest.

References

1. Guo, L.; Yang, Z.; Lin, F. A Novel Strategy for Sensorless Control of IPMSM with Error Compensation Based on Rotating High Frequency Carrier Signal Injection. *Energies* **2020**, *13*, 1919. [CrossRef]
2. Kumar, P.; Bottesi, O.; Calligaro, S.; Alberti, L.; Petrella, R. Self-Adaptive High-Frequency Injection Based Sensorless Control for Interior Permanent Magnet Synchronous Motor Drives. *Energies* **2019**, *12*, 3645. [CrossRef]
3. Szalay, I.; Fodor, D.; Enisz, K.; Medve, H. Permanent Magnet Synchronous Motor Model Extension for High-Frequency Signal Injection-Based Sensorless Magnet Polarity Detection. *Energies* **2022**, *15*, 1131. [CrossRef]
4. Yu, K.; Wang, Z.; Li, L. An Optimized Time Sequence for Sensorless Control of IPMSM Drives via High-Frequency Square-Wave Signal Injection Scheme. *Energies* **2022**, *15*, 2246. [CrossRef]
5. Tian, L.; Zhao, J.; Sun, J. Sensorless Control of Interior Permanent Magnet Synchronous Motor in Low-Speed Region Using Novel Adaptive Filter. *Energies* **2016**, *9*, 1084. [CrossRef]
6. Urbanski, K.; Janiszewski, D. Position Estimation at Zero Speed for PMSMs Using Artificial Neural Networks. *Energies* **2021**, *14*, 8134. [CrossRef]
7. Wang, S.; Zhao, J.; Yang, K. High Frequency Square-Wave Voltage Injection Scheme-Based Position Sensorless Control of IPMSM in the Low- and Zero- Speed Range. *Energies* **2019**, *12*, 4776. [CrossRef]
8. Alaei, A.; Nejad, S.M.S.; Gieras, J.F.; Lee, D.; Ahn, J. Reduction of high-frequency injection losses, acoustic noise and total harmonic distortion in IPMSM sensorless drives. *IET Power Electron.* **2019**, *12*, 3197–3207. [CrossRef]
9. Pando-Acedo, J.; Romero-Cadaval, E.; Milanes-Montero, M.I.; Barrero-Gonzalez, F. Improvements on a Sensorless Scheme for a Surface-Mounted Permanent Magnet Synchronous Motor Using Very Low Voltage Injection. *Energies* **2020**, *13*, 2732. [CrossRef]
10. Ha, J.-I.; Ide, K.; Sawa, T.; Sul, S.-K. Sensorless rotor position estimation of an interior permanent-magnet motor from initial states. *IEEE Trans. Ind. Appl.* **2003**, *39*, 761–767. [CrossRef]
11. Jansen, P.; Lorenz, R. Transducerless position and velocity estimation in induction and salient AC machines. *IEEE Trans. Ind. Appl.* **1995**, *31*, 240–247. [CrossRef]
12. Imai, N.; Morimoto, S.; Sanada, M.; Takeda, Y. 3-phase High Frequency Voltage Input Sensorless Control for Hybrid Electric Vehicle Applications. *World Electr. Veh. J.* **2007**, *1*, 279–285. [CrossRef]
13. Jung, T.-U.; Jang, J.-H.; Park, C.-S. A Back-EMF Estimation Error Compensation Method for Accurate Rotor Position Estimation of Surface Mounted Permanent Magnet Synchronous Motors. *Energies* **2017**, *10*, 1160. [CrossRef]
14. Chen, G.-R.; Yang, S.-C.; Hsu, Y.-L.; Li, K. Position and Speed Estimation of Permanent Magnet Machine Sensorless Drive at High Speed Using an Improved Phase-Locked Loop. *Energies* **2017**, *10*, 1571. [CrossRef]
15. You, Z.-C.; Yang, S.-M. A Restarting Strategy for Back-EMF-Based Sensorless Permanent Magnet Synchronous Machine Drive. *Energies* **2019**, *12*, 1818. [CrossRef]
16. Chen, Z.; Tomita, M.; Doki, S.; Okuma, S. An extended electromotive force model for sensorless control of interior permanent-magnet synchronous motors. *IEEE Trans. Ind. Electron.* **2003**, *50*, 288–295. [CrossRef]
17. Wang, G.; Ding, L.; Li, Z.; Xu, J.; Zhang, G.; Zhan, H.; Ni, R.; Xu, D. Enhanced Position Observer Using Second-Order Generalized Integrator for Sensorless Interior Permanent Magnet Synchronous Motor Drives. *IEEE Trans. Energy Convers.* **2014**, *29*, 486–495. [CrossRef]
18. Kim, J.; Jeong, I.; Nam, K.; Yang, J.; Hwang, T. Sensorless Control of PMSM in a High-Speed Region Considering Iron Loss. *IEEE Trans. Ind. Electron.* **2015**, *62*, 6151–6159. [CrossRef]
19. Jiang, F.; Yang, F.; Sun, S.; Yang, K. Static-Errorless Rotor Position Estimation Method Based on Linear Extended State Observer for IPMSM Sensorless Drives. *Energies* **2022**, *15*, 1943. [CrossRef]
20. Du, B.; Wu, S.; Han, S.; Cui, S. Application of Linear Active Disturbance Rejection Controller for Sensorless Control of Internal Permanent-Magnet Synchronous Motor. *IEEE Trans. Ind. Electron.* **2016**, *63*, 3019–3027. [CrossRef]
21. Qu, L.; Qiao, W.; Qu, L. An Enhanced Linear Active Disturbance Rejection Rotor Position Sensorless Control for Permanent Magnet Synchronous Motors. *IEEE Trans. Power Electron.* **2019**, *35*, 6175–6184. [CrossRef]

22. Cho, Y. Improved Sensorless Control of Interior Permanent Magnet Sensorless Motors Using an Active Damping Control Strategy. *Energies* **2016**, *9*, 135. [CrossRef]
23. Moradian, M.; Soltani, J.; Benbouzid, M.; Najjar-Khodabakhsh, A. A Parameter Independent Stator Current Space-Vector Reference Frame-Based Sensorless IPMSM Drive Using Sliding Mode Control. *Energies* **2021**, *14*, 2365. [CrossRef]
24. Hoai, H.-K.; Chen, S.-C.; Than, H. Realization of the Sensorless Permanent Magnet Synchronous Motor Drive Control System with an Intelligent Controller. *Electronics* **2020**, *9*, 365. [CrossRef]
25. Yin, Q.; Li, H.; Luo, H.; Wang, Q.; Xu, C. An Improved Sensorless Vector Control Method for IPMSM Drive with Small DC-Link Capacitors. *Energies* **2020**, *13*, 580. [CrossRef]
26. Chen, J.; Chen, S.; Wu, X.; Tan, G.; Hao, J. A Super-Twisting Sliding-Mode Stator Flux Observer for Sensorless Direct Torque and Flux Control of IPMSM. *Energies* **2019**, *12*, 2564. [CrossRef]
27. Bao, D.; Wu, H.; Wang, R.; Zhao, F.; Pan, X. Full-Order Sliding Mode Observer Based on Synchronous Frequency Tracking Filter for High-Speed Interior PMSM Sensorless Drives. *Energies* **2020**, *13*, 6511. [CrossRef]
28. Wang, Y.; Wang, X.; Xie, W.; Dou, M. Full-Speed Range Encoderless Control for Salient-Pole PMSM with a Novel Full-Order SMO. *Energies* **2018**, *11*, 2423. [CrossRef]
29. Chi, S.; Zhang, Z.; Xu, L. Sliding-Mode Sensorless Control of Direct-Drive PM Synchronous Motors for Washing Machine Applications. *IEEE Trans. Ind. Appl.* **2009**, *45*, 582–590. [CrossRef]
30. Liu, Z.; Chen, W. Research on an Improved Sliding Mode Observer for Speed Estimation in Permanent Magnet Synchronous Motor. *Processes* **2022**, *10*, 1182. [CrossRef]
31. Kim, H.; Son, J.; Lee, J. A High-Speed Sliding-Mode Observer for the Sensorless Speed Control of a PMSM. *IEEE Trans. Ind. Electron.* **2011**, *58*, 4069–4077. [CrossRef]
32. Qiao, Z.; Shi, T.; Wang, Y.; Yan, Y.; Xia, C.; He, X. New Sliding-Mode Observer for Position Sensorless Control of Permanent-Magnet Synchronous Motor. *IEEE Trans. Ind. Electron.* **2012**, *60*, 710–719. [CrossRef]
33. An, Q.; Zhang, J.; An, Q.; Liu, X.; Shamekov, A.; Bi, K. Frequency-Adaptive Complex-Coefficient Filter-Based Enhanced Sliding Mode Observer for Sensorless Control of Permanent Magnet Synchronous Motor Drives. *IEEE Trans. Ind. Appl.* **2019**, *56*, 335–343. [CrossRef]
34. Liang, D.; Li, J.; Qu, R. Sensorless Control of Permanent Magnet Synchronous Machine Based on Second-Order Sliding-Mode Observer with Online Resistance Estimation. *IEEE Trans. Ind. Appl.* **2017**, *53*, 3672–3682. [CrossRef]
35. Liu, Y.; Fang, J.; Tan, K.; Huang, B.; He, W. Sliding Mode Observer with Adaptive Parameter Estimation for Sensorless Control of IPMSM. *Energies* **2020**, *13*, 5991. [CrossRef]
36. Zhao, Y.; Yu, H.; Wang, S. An Improved Super-Twisting High-Order Sliding Mode Observer for Sensorless Control of Permanent Magnet Synchronous Motor. *Energies* **2021**, *14*, 6047. [CrossRef]
37. Kyslan, K.; Petro, V.; Bober, P.; Šlapák, V.; Ďurovský, F.; Dybkowski, M.; Hric, M. A Comparative Study and Optimization of Switching Functions for Sliding-Mode Observer in Sensorless Control of PMSM. *Energies* **2022**, *15*, 2689. [CrossRef]
38. Cui, J.; Xing, W.; Qin, H.; Hua, Y.; Zhang, X.; Liu, X. Research on Permanent Magnet Synchronous Motor Control System Based on Adaptive Kalman Filter. *Appl. Sci.* **2022**, *12*, 4944. [CrossRef]
39. Dilys, J.; Stankevič, V.; Łuksza, K. Implementation of Extended Kalman Filter with Optimized Execution Time for Sensorless Control of a PMSM Using ARM Cortex-M3 Microcontroller. *Energies* **2021**, *14*, 3491. [CrossRef]
40. Shahzad, K.; Jawad, M.; Ali, K.; Akhtar, J.; Khosa, I.; Bajaj, M.; Elattar, E.E.; Kamel, S. A Hybrid Approach for an Efficient Estimation and Control of Permanent Magnet Synchronous Motor with Fast Dynamics and Practically Unavailable Measurements. *Appl. Sci.* **2022**, *12*, 4958. [CrossRef]
41. Urbanski, K.; Janiszewski, D. Sensorless Control of the Permanent Magnet Synchronous Motor. *Sensors* **2019**, *19*, 3546. [CrossRef] [PubMed]
42. Ortega, R.; Praly, L.; Astolfi, A.; Lee, J.; Nam, K. Estimation of Rotor Position and Speed of Permanent Magnet Synchronous Motors With Guaranteed Stability. *IEEE Trans. Control Syst. Technol.* **2010**, *19*, 601–614. [CrossRef]
43. Lee, J.; Hong, J.; Nam, K.; Ortega, R.; Praly, L.; Astolfi, A. Sensorless Control of Surface-Mount Permanent-Magnet Synchronous Motors Based on a Nonlinear Observer. *IEEE Trans. Power Electron.* **2009**, *25*, 290–297. [CrossRef]
44. Bobtsov, A.A.; Pyrkin, A.A.; Ortega, R.; Vukosavic, S.N.; Stankovic, A.M.; Panteley, E.V. A robust globally convergent position observer for the permanent magnet synchronous motor. *Automatica* **2015**, *61*, 47–54. [CrossRef]
45. Choi, J.; Nam, K.; Bobtsov, A.A.; Pyrkin, A.; Ortega, R. Robust Adaptive Sensorless Control for Permanent-Magnet Synchronous Motors. *IEEE Trans. Power Electron.* **2016**, *32*, 3989–3997. [CrossRef]
46. Marchesoni, M.; Passalacqua, M.; Vaccaro, L.; Calvini, M.; Venturini, M. Low Speed Performance Improvement in a Self-Commissioned Sensorless PMSM Drive Based on Rotor Flux Observer. In Proceedings of the 2019 21st European Con-ference on Power Electronics and Applications (EPE '19 ECCE Europe), Genova, Italy, 3–5 September 2019; pp. 1–10.
47. Marchesoni, M.; Passalacqua, M.; Vaccaro, L.; Calvini, M.; Venturini, M. An Improved Low-Noise Sensorless PMSM Drive able to Face Highly Intermittent Load Torque. In Proceedings of the 2019 IEEE 10th International Symposium on Sensorless Control for Electrical Drives (SLED), Turin, Italy, 9–10 September 2019; pp. 1–6.
48. Marchesoni, M.; Passalacqua, M.; Vaccaro, L.; Calvini, M.; Venturini, M. Performance improvement in a sensorless surface-mounted PMSM drive based on rotor flux observer. *Control Eng. Pract.* **2019**, *96*, 104276. [CrossRef]

49. Carbone, L.; Cosso, S.; Marchesoni, M.; Passalacqua, M.; Vaccaro, L. State-Space Approach for SPMSM Sensorless Passive Algorithm Tuning. *Energies* **2021**, *14*, 7180. [CrossRef]
50. Choi, J.; Nam, K.; Bobtsov, A.A.; Ortega, R. Sensorless Control of IPMSM Based on Regression Model. *IEEE Trans. Power Electron.* **2018**, *34*, 9191–9201. [CrossRef]
51. Choi, J. Regression Model-Based Flux Observer for IPMSM Sensorless Control with Wide Speed Range. *Energies* **2021**, *14*, 6249. [CrossRef]
52. Mubarok, M.S.; Liu, T.-H.; Tsai, C.-Y.; Wei, Z.-Y. A Wide-Adjustable Sensorless IPMSM Speed Drive Based on Current Deviation Detection under Space-Vector Modulation. *Energies* **2020**, *13*, 4431. [CrossRef]
53. Wang, B.; Wang, Y.; Feng, L.; Jiang, S.; Wang, Q.; Hu, J. Permanent-Magnet Synchronous Motor Sensorless Control Using Proportional-Integral Linear Observer with Virtual Variables: A Comparative Study with a Sliding Mode Observer. *Energies* **2019**, *12*, 877. [CrossRef]
54. Benevieri, A.; Marchesoni, M.; Passalacqua, M.; Vaccaro, L. Experimental Low-Speed Performance Evaluation and Comparison of Sensorless Passive Algorithms for SPMSM. *IEEE Trans. Energy Convers.* **2021**, *37*, 654–664. [CrossRef]